ELSEVIER

Applied Catalysis A: General 212 (2001) 17–60

APPLIED CATALYSIS A: GENERAL

www.elsevier.com/locate/apcata

Mechanisms of catalyst deactivation

Calvin H. Bartholomew*

Department of Chemical Engineering, Brigham Young University, Provo, UT 84602, USA

Abstract

The literature treating mechanisms of catalyst deactivation is reviewed. Intrinsic mechanisms of catalyst deactivation are many; nevertheless, they can be classified into six distinct types: (i) poisoning, (ii) fouling, (iii) thermal degradation, (iv) vapor compound formation accompanied by transport, (v) vapor-solid and/or solid-solid reactions, and (vi) attrition/crushing. As (i), (iv), and (v) are chemical in nature and (ii) and (v) are mechanical, the causes of deactivation are basically three-fold: chemical, mechanical and thermal. Each of these six mechanisms is defined and its features are illustrated by data and examples from the literature. The status of knowledge and needs for further work are also summarized for each type of deactivation mechanism. The development during the past two decades of more sophisticated surface spectroscopies and powerful computer technologies provides opportunities for obtaining substantially better understanding of deactivation mechanisms and building this understanding into comprehensive mathematical models that will enable more effective design and optimization of processes involving deactivating catalysts.

*K*eywords: Catalyst: deactivation, degradation, fouling, poisoning, sintering, and mechanical degradation of; Catalyst deactivation by: coke and carbon formation, vapor compound formation, vapor-solid and solid-solid reactions, attrition and crushing; Mechanisms of: catalyst deactivation, fouling, poisoning, sintering, vapor-solid and solid-solid reactions, and mechanical degradation; Research opportunities and needs: mechanisms of catalyst deactivation, fouling, poisoning, sintering, vapor-solid and solid-solid reactions, and mechanical degradation; Technical knowledge status of: mechanisms of catalyst deactivation, fouling, poisoning, sintering, vapor-solid and solid-solid reactions, and mechanical degradation

1. Introduction

Catalyst deactivation, the loss over time of catalytic activity and/or selectivity, is a problem of great and continuing concern in the practice of industrial catalytic processes. Costs to industry for catalyst replacement and process shutdown total billions of dollars per year. Time scales for catalyst deactivation vary considerably; for example, in the case of cracking catalysts, catalyst mortality may be in the order of seconds, while in ammonia synthesis the iron catalyst may last for 5–10 years. But it is inevitable that all catalysts will decay.

Typically, the loss of activity in a well-controlled process occurs slowly. However, process upsets or poorly designed hardware can bring about catastrophic failure. For example, in steam reforming of methane or naphtha great care must be taken to avoid reactor operation at excessively high temperatures or at steam to hydrocarbon ratios below a critical value. Indeed, these conditions can cause formation of large quantities of carbon filaments which plug catalyst pores and voids, pulverize catalyst pellets, and bring about process shut down all within a few hours.

While catalyst deactivation is inevitable for most processes, some of its immediate, drastic consequences may be avoided, postponed, or even reversed. Thus, deactivation issues (i.e. extent, rate and reactivation) greatly impact research, development, design,

* Fax: +1-801-378-4162.
E-mail address: bartc@byu.edu (C.H. Bartholomew).

0926-860X/01/$ – see front matter
PII: S0926-860X(00)00843-7

and operation of commercial processes. Accordingly, there is considerable motivation to understand and treat catalyst decay. Indeed, over the past three decades, the science of catalyst deactivation has been steadily developing, while literature addressing this topic has expanded considerably to include books [1–4]; comprehensive reviews [5–8]; and proceedings of international symposia [9–14]. A significant fraction of this literature addresses mechanisms of deactivation. This area of research provides a critical understanding which is the foundation for modeling deactivation processes, designing stable catalysts, and optimizing processes to prevent or slow catalyst deactivation.

This review summarizes the present state of knowledge regarding mechanisms of catalyst decay. Areas of mechanistic research in which further investigations are needed are also addressed.

2. Mechanisms of deactivation

Prevention of catalyst degradation poses substantial challenges in the design and operation of a large-scale, catalytic process. There are many paths for catalyst decay. For example, a catalyst may be poisoned by any one of a dozen contaminants present in the feed; its surface, pores and voids may be fouled by carbon or coke produced by cracking/condensation reactions of hydrocarbon reactants, intermediates and/or products. In the treatment of a power plant flue gas, the catalyst can be dusted or eroded by and/or plugged with fly ash. Catalytic converters used to reduce emissions from gasoline or diesel engines may be poisoned or fouled by fuel or lubricant additives and/or engine corrosion products. If the catalytic reaction is conducted at high temperatures, thermal degradation may occur in the form of active phase crystallite growth, collapse of the carrier (support) pore structure and/or solid-state reactions of the active phase with the carrier or promoters. In addition, the presence of oxygen or chlorine in the feed gas can lead to formation of volatile oxides or chlorides of the active phase followed by gas phase transport from the reactor. Similarly, changes in the oxidation state of the active catalytic phase can be induced by the presence of reactive gases in the feed.

Thus, the mechanisms of catalyst deactivation are many; nevertheless, they can be grouped into six intrinsic mechanisms of catalyst decay: (i) poisoning, (ii) fouling, (iii) thermal degradation, (iv) vapor compound formation accompanied by transport, (v) vapor–solid and/or solid–solid reactions, and (vi) attrition/crushing. As (i), (iv), and (v) are chemical in nature while (ii) and (v) are mechanical, the causes of deactivation are basically three-fold: chemical, mechanical and thermal. Each of the six basic mechanisms is defined briefly in Table 1 and treated in some detail in the subsections which follow with an emphasis on the first three. Mechanisms (iv) and (v) are treated together, since (iv) is a subset of (v).

2.1. Poisoning

Poisoning [3,15–21] is the strong chemisorption of reactants, products or impurities on sites otherwise

Table 1
Mechanisms of catalyst deactivation

Mechanism	Type	Brief definition/description
Poisoning	Chemical	Strong chemisorption of species on catalytic sites, thereby blocking sites for catalytic reaction
Fouling	Mechanical	Physical deposition of species from fluid phase onto the catalytic surface and in catalyst pores
Thermal degradation	Thermal	Thermally induced loss of catalytic surface area, support area, and active phase–support reactions
Vapor formation	Chemical	Reaction of gas with catalyst phase to produce volatile compound
Vapor–solid and solid–solid reactions	Chemical	Reaction of fluid, support, or promoter with catalytic phase to produce inactive phase
Attrition/crushing	Mechanical	Loss of catalytic material due to abrasion
		Loss of internal surface area due to mechanical-induced crushing of the catalyst particle

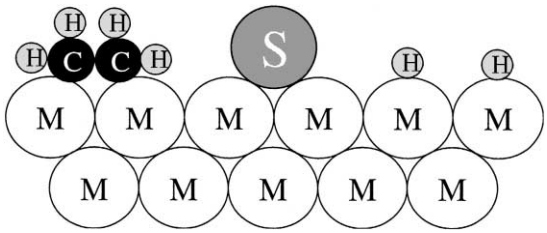

Fig. 1. Conceptual model of poisoning by sulfur atoms of a metal surface during ethylene hydrogenation.

available for catalysis. Thus, poisoning has operational meaning; that is, whether a species acts as a poison depends upon its adsorption strength relative to the other species competing for catalytic sites. For example, oxygen can be a reactant in partial oxidation of ethylene to ethylene oxide on a silver catalyst and a poison in hydrogenation of ethylene on nickel. In addition to physically blocking of adsorption sites, adsorbed poisons may induce changes in the electronic or geometric structure of the surface [16,20].

Mechanisms by which a poison may affect catalytic activity are multifold as illustrated by a conceptual two-dimensional model of sulfur poisoning of ethylene hydrogenation on a metal surface shown in Fig. 1. To begin with, a strongly adsorbed atom of sulfur physically blocks at least one three- or four-fold adsorption/reaction site (projecting into three dimensions) and three or four topside sites on the metal surface. Second, by virtue of its strong chemical bond, it electronically modifies its nearest neighbor metal atoms and possibly its next nearest neighbor atoms, thereby modifying their abilities to adsorb and/or dissociate reactant molecules (in this case H_2 and ethylene molecules), although these effects do not extend beyond about 5 a.u. [20]. A third effect may be the restructuring of the surface by the strongly adsorbed poison, possibly causing dramatic changes in catalytic properties, especially for reactions sensitive to surface structure. In addition, the adsorbed poison blocks access of adsorbed reactants to each other (a fourth effect) and finally prevents or slows the surface diffusion of adsorbed reactants (a fifth effect).

Catalyst poisons can be classified according to their chemical makeup, selectivity for active sites and the types of reactions poisoned. Table 2 lists four groups of catalyst poisons classified according to chemical origin and their type of interaction with metals. It should be emphasized that interactions of group VA–VIIIA elements with catalytic metal phases depend on the oxidation state of the former, i.e. how many electron pairs are available for bonding and the degree of shielding of the sulfur ion by ligands [15]. Thus, the order of decreasing toxicity for poisoning of a given metal by different sulfur species is H_2S, SO_2, SO_4^{2-}, i.e. in the order of increased shielding by oxygen. Toxicity increases with increasing atomic or molecular size and electronegativity, but decreases if the poison can be gasified by O_2, H_2O or H_2 present in the reactant stream [20]; for example, adsorbed carbon can be gasified by O_2 to CO or CO_2 or by H_2 to CH_4.

Table 3 lists a number of common poisons for selected catalysts in important representative reactions. It is apparent that organic bases (e.g. amines) and ammonia are common poisons for acidic solids such as silica-alumina and zeolites in cracking and hydrocracking reactions while sulfur- and arsenic-containing compounds are typical poisons for metals in hydrogenation, dehydrogenation and steam reforming reactions. Metal compounds (e.g. Ni, Pb, V and Zn) are poisons in automotive emissions control, catalytic cracking and hydrotreating. Acetylene is a poison for ethylene oxidation, while asphaltenes are poisons in hydrotreating of petroleum residual.

Poisoning selectivity is illustrated in Fig. 2, a plot of activity (the reaction rate normalized to initial rate)

Table 2
Common poisons classified according to chemical structure

Chemical type	Examples	Type of interaction with metals
Groups VA and VIA	N, P, As, Sb, O, S, Se, Te	Through s- and p-orbitals; shielded structures are less toxic
Group VIIA	F, Cl, Br, I	Through s- and p-orbitals; formation of volatile halides
Toxic heavy metals and ions	As, Pb, Hg, Bi, Sn, Zn, Cd, Cu, Fe	Occupy d-orbitals; may form alloys
Molecules which adsorb with multiple bonds	CO, NO, HCN, benzene, acetylene, other unsaturated hydrocarbons	Chemisorption through multiple bonds and back bonding

Table 3
Poisons for selected catalysts in important representative reactions

Catalyst	Reaction	Poisons
Silica-alumina, zeolites	Cracking	Organic bases, hydrocarbons heavy metals
Nickel, platinum, palladium	Hydrogenation dehydrogenation	Compounds of S, P, As, Zn, Hg, halides, Pb, NH_3, C_2H_2
Nickel	Steam reforming of methane, naphtha	H_2S, As
Iron, ruthenium	Ammonia synthesis	O_2, H_2O, CO, S, C_2H_2, H_2O
Cobalt, and iron	Fischer–Tropsch synthesis	H_2S, COS, As, NH_3, metal carbonyls
Noble metals on zeolites	Hydrocracking	NH_3, S, Se, Te, P
Silver	Ethylene oxidation to ethylene oxide	C_2H_2
Vanadium oxide	Oxidation selective catalytic reduction	As, Fe, K, Na from fly ash
Platinum, palladium	Oxidation of CO and hydrocarbons	Pb, P, Zn, SO_2, Fe
Cobalt and molybdenum sulfides	Hydrotreating of residue	Asphaltenes, N compounds, Ni, V

versus normalized poison concentration. "Selective" poisoning involves preferential adsorption of the poison on the most active sites at low concentrations. If sites of lesser activity are blocked initially, the poisoning is "anti-selective". If the activity loss is proportional to the concentration of adsorbed poison, the poisoning is "non-selective". An example of selective poisoning is the deactivation of platinum by CO for the *para*-H_2 conversion (Fig. 3a; [22]) while Pb poisoning of CO oxidation on platinum is apparently anti-selective (Fig. 3b; [23]), and arsenic poisoning of cyclopropane hydrogenation on Pt is non-selective (Fig. 3c; [24]). For non-selective poisoning the linear decrease in activity with poison concentration or susceptibility (σ) is defined by the slope of the activity versus poison concentration curve. Several other important terms associated with poisoning are defined in Table 4. Poison tolerance, the activity at saturation coverage of the poison and resistance, the inverse of deactivation rate, are important concepts that are often encountered in discussions of poisoning including those below.

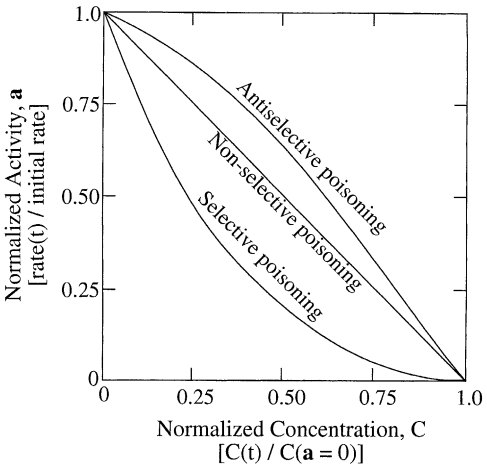

Fig. 2. Three kinds of poisoning behavior in terms of normalized activity vs. normalized poison concentration (courtesy: Kluwer Academic Publishers).

The activity versus poison concentration patterns illustrated in Fig. 2 are based on the assumption of uniform poisoning of the catalyst surface and surface reaction rate controlling, i.e. negligible pore diffusional resistance. These assumptions, however, are rarely met in typical industrial processes because the severe reaction conditions of high temperature and high pressure bring about a high pore diffusional resistance for either the main or poisoning reaction or both. In physical terms, this means that the reaction may occur preferentially in the outer shell of the catalysts particle, or that poison is preferentially adsorbed in the outer shell of the catalyst particle, or both. The non-uniformly distributed reaction and/or poison leads to non-linear activity versus poison concentration curves which mimic the patterns in Fig. 2 but are not truly selective or anti-selective poisoning. For example, if the main reaction is limited to an outer shell in a pellet where poison is concentrated, the drop in activity with concentration will be precipitous. The effects of pore diffusional effects in poisoning (non-uniform poison) are treated elsewhere [2,4,6–8,17].

As sulfur poisoning is a difficult problem in many important catalytic processes (e.g. hydrogenation, methanation, Fischer–Tropsch synthesis, steam reforming and fuel cell power production), it merits separate discussion as an example of catalyst poisoning

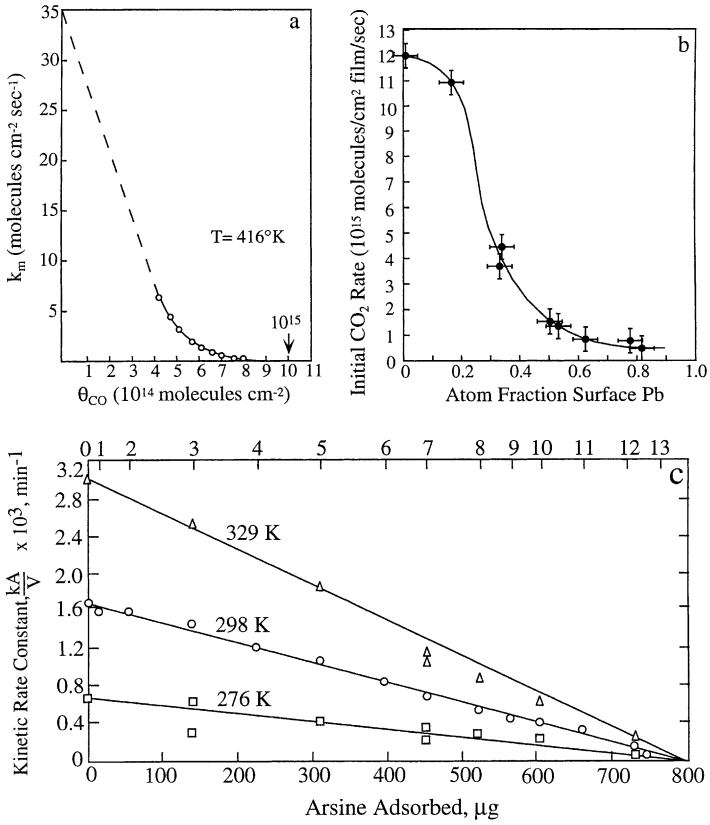

Fig. 3. (a) CO poisoning of *para*-H_2 conversion over a Pt foil [22]; (b) effect of lead coverage on the rate of CO oxidation of Pt film [23]; (c) rate constants of cyclopropane hydrogenolysis over a Pt film as a function of the amount of AsH_3 adsorbed [24] (courtesy: Kluwer Academic Publishers).

phenomena. Studies of sulfur poisoning in hydrogenation and CO hydrogenation reactions have been thoroughly reviewed [8,20,25–29]. Much of the previous work focused on poisoning of nickel metal catalysts by H_2S, the primary sulfur poison in many important catalytic processes, and thus provides some useful case studies of poisoning.

Previous adsorption studies [26,28] indicate that H_2S adsorbs strongly and dissociatively on nickel metal surfaces. The high stability and low reversibility

Table 4
Important poisoning parameters

Parameter	Definition
Activity (a)	Reaction rate at time t relative to that at $t = 0$
Susceptibility (σ)	Negative slope of the activity vs. poison concentration curve ($\sigma = (a - 1)/C(t)$); measure of a catalyst's sensitivity to a given poison
Toxicity	Susceptibility of a given catalyst for a poison relative to that for another poison
Resistance	Inverse of the deactivation rate; property which determines how rapidly a catalyst deactivates
Tolerance ($a(C_{sat})$)	Activity of the catalyst at saturation coverage (many catalysts may have negligible activity at saturation coverage)

of adsorbed sulfur is illustrated by the data in Fig. 4 [26], in which most of the previous equilibrium data for nickel are represented on a single plot of $\log(P_{H_2S}/P_{H_2})$ versus reciprocal temperature. The solid line corresponds to the equilibrium data for formation of bulk Ni_3S_2. Based on the equation $\Delta G^0 = RT\ln(P_{H_2S}/P_{H_2}) = \Delta H - T\,\Delta S$, the slope of this line is $\Delta H/R$, where $\Delta H = -75$ kJ/mol and the intercept is $-\Delta S/R$. Most of the adsorption data lie between the dashed lines corresponding to $\Delta H = -125$ and -165 kJ/mol for coverages ranging from 0.5 to 0.9, indicating that adsorbed sulfur is more stable than the bulk sulfide. Indeed, extrapolation of high temperature data to zero coverage using a Tempkin isotherm [27] yields an enthalpy of adsorption of -250 kJ/mol; in other words, at low sulfur coverages, surface nickel–sulfur bonds are a factor of three more stable than bulk nickel–sulfur bonds. It is apparent from Fig. 4 that the absolute heat of adsorption increases with decreasing coverage and that the equilibrium partial pressure of H_2S increases with increasing temperature and increasing coverage. For instance, at 725 K (450°C) and $\theta = 0.5$, the values of P_{H_2S}/P_{H_2} range from about 10^{-8} to 10^{-9}.

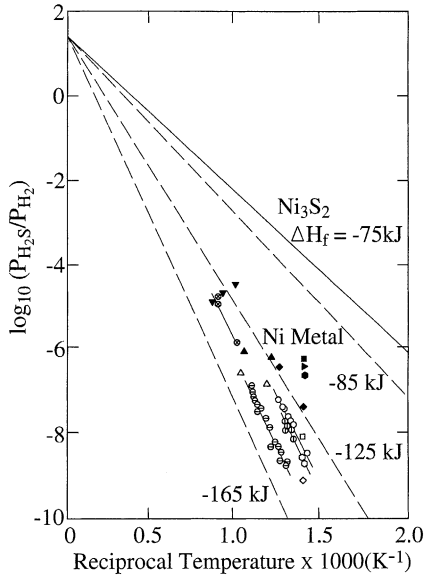

Fig. 4. Equilibrium partial pressure of H_2S vs. reciprocal temperature (values of ΔH_f based on 1 mol of H_2S); open symbols, $\theta = 0.5$–0.6; closed symbols, $\theta = 0.8$–0.9 [26] (courtesy: Academic Press).

In other words, half coverage occurs at 1–10 ppb H_2S, a concentration range at the lower limit of our present analytical capability! At the same temperature (450°C) almost complete coverage ($\theta > 0.9$) occurs at values of P_{H_2S}/P_{H_2} of 10^{-7}–10^{-6} (0.1–1 ppm) or at H_2S concentrations encountered in many catalytic processes after the gas has been processed to remove sulfur compounds. These data are typical of sulfur adsorption on most catalytic metals. Thus, we can expect that H_2S (and other sulfur impurities) will adsorb essentially irreversibly to high coverage in most catalytic processes involving metal catalysts.

Two important keys to reaching a deeper understanding of poisoning phenomena include: (1) determining surface structures of poisons adsorbed on metal surfaces and (2) understanding how surface structure and hence adsorption stoichiometry change with increasing coverage of the poison. Studies of structures of adsorbed sulfur on single crystal metals (especially Ni) [26,30–34] provide such information. They reveal, for example, that sulfur adsorbs on Ni(1 0 0) in an ordered P(2 × 2) overlayer, bonded to four Ni atoms at $S/Ni_s < 0.25$ and in a C(2 × 2) overlayer to two Ni atoms for $S/Ni_s = 0.25$–0.50 (see Fig. 5; Ni_s denotes a surface atom of Ni); saturation coverage of sulfur on Ni occurs at $S/Ni_s = 0.5$. Adsorption of sulfur on Ni(1 1 0), Ni(1 1 1) and higher index planes of Ni is more complicated; while the same P(2 × 2) structure is observed at low coverage, complex overlayers appear at higher coverages, for example, on Ni(1 1 1) in two additional stages (structures) up to saturation at $S/Ni_s = 0.5$. In more open surface structures such as Ni(1 1 0) and Ni(2 1 0), saturation coverage occurs at $S/Ni_s = 0.74$ and 1.09, respectively; indeed, there is a trend of increasing S/Ni_s with decreasing planar density for Ni while the saturation sulfur concentration remains constant at 44 ng/cm^2 Ni (see Table 5).

Reported saturation stoichiometries for sulfur adsorption on polycrystalline and supported Ni catalysts vary from $S/Ni_s = 0.25$ to 1.3 [26]. The values of saturation coverage greater than $S/Ni_s = 0.5$ may be explained by (1) a higher fraction of adsorption on sites of lower coordination number, i.e. involving more open planes or intersections of planes; (2) adsorption at higher gas phase concentrations of H_2S in line with the observed trend of increasing saturation coverage with increasing H_2S concentration in Figs. 4 and 6; and/or (3) reconstruction of the

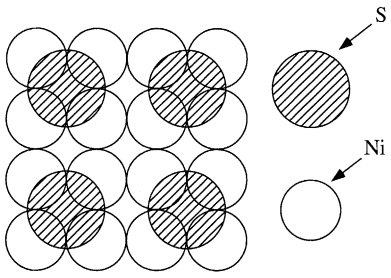

(a) p (2x2), $S/Ni_S = 0.25$

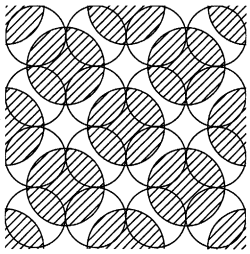

(b) c (2x2), $S/Ni_S = 0.5$

Fig. 5. Schematic view of sulfur adsorbed on a Ni(1 0 0) surface at (a) $S/Ni_s = 0.25$ in a P(2 × 2) structure and (b) $S/Ni_s = 0.50$ in a C(2 × 2) structure.

surface by adsorbed sulfur at higher adsorption temperatures. The first effect would be favored, and in fact is observed, for supported catalysts of higher dispersion [26]. The second effect may explain the typically lower observed values of S/Ni_s for single crystal Ni which are measured at extremely low pressures (high vacuum) relative to the higher values of S/Ni_s for polycrystalline and supported Ni, typically measured at orders of magnitude higher pressure; in the case of the single crystal work the surface is not in equilibrium with gas phase H_2S/H_2.

The third effect, reconstruction of nickel surfaces by adsorbed sulfur, has been reported by a number of workers [26]; for example, Edmonds and co-workers [33,34] found that sulfur adsorbed at near saturation coverage on a Ni(1 1 1) face was initially in a hexagonal pattern but upon heating above 700 K reoriented to a distorted C(2 × 2) structure on a Ni(1 0 0) layer. In another study [31], sulfur adsorbed on a Ni(8 1 0) caused decomposition to (1 0 0) and (4 1 0) facets. Based on their review of the reconstruction studies, Bartholomew et al. [26] concluded that at high temperatures and near saturation coverages, restructuring by sulfur of different facets of Ni to the more stable Ni(1 0 0) is probably a general phenomenon. If so, the S/Ni_s ratio at saturation would in principle be 0.5 for the reconstructed surface. In the first example above, restructuring would not affect the S/Ni_s ratio at saturation, since it is 0.5 for both (1 0 0) and (1 1 1) planes; however, in the second example, the S/Ni_s ratio at saturation would probably decrease, as rough planes transform to smoother ones. Nevertheless, the possibility of increases in the S/Ni_s ratio at saturation due to reconstruction cannot be ruled out.

In the previous discussion of Fig. 4, it was observed that $-\Delta H_{ads}$ decreases with increasing sulfur coverage; data in Fig. 6 from Hepola et al. [35] show that $-\Delta H_{ads}$ decreases with increasing gas phase H_2S concentration and coverage. However, in contrast to the data in Fig. 4, those in Fig. 6 [35] show that at very high H_2S concentrations and high adsorption temperatures, $-\Delta H_{ads}$ falls well below the $-\Delta H_{formation}$ of bulk Ni_3S_2; at the same time the S/Ni_s ratio approaches that of Ni_2S_3. This is a unique result, since all of the data obtained at lower temperatures and H_2S concentrations [26] show $-\Delta H_{ads}$ to be greater than $-\Delta H_{formation}$ of Ni_3S_2.

Table 5
Sulfur adsorption densities on various crystal faces of nickel[a]

Crystal face	Sulfur concentration at saturation (ng S/cm^2)	Number of S atoms/cm^2 ($\times 10^{15}$)	Number of Ni atoms/cm^2 ($\times 10^{15}$)	S atoms per surface Ni atoms
(1 1 1)	47 ± 1	0.86	1.8	0.48
(1 0 0)	43 ± 1	0.80	1.6	0.50
(1 1 0)	44.5 ± 1	0.82	1.1	0.74
(2 1 0)	42 ± 1	0.78	0.72	1.09
Polycrystalline	44.5 ± 1	0.82	–	–

[a] Data from [30].

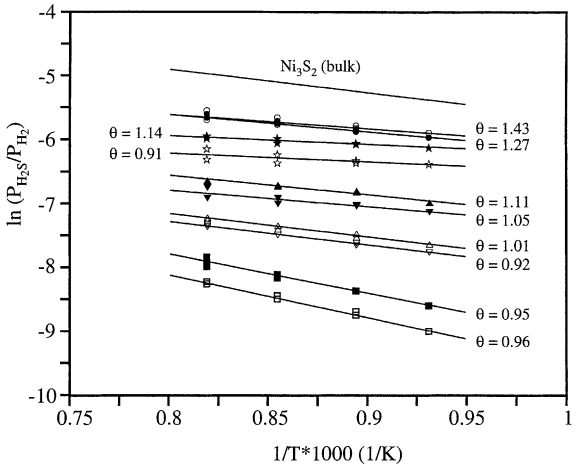

Fig. 6. Sulfur chemisorption isosteres on a Ni/α-Al_2O_3 catalyst at high temperatures and high H_2S concentrations [35].

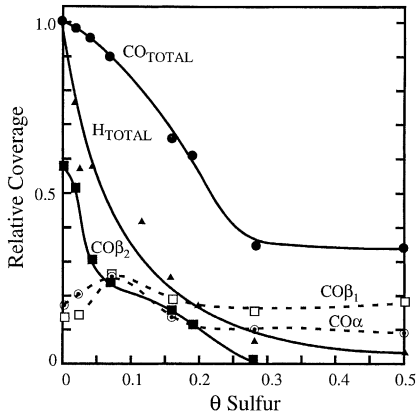

Fig. 7. Area under thermal programmed desorption spectra for H_2 and the α, β_1, β_2, and total CO adsorption curves as a function of sulfur pre-coverage [38].

From the above discussion, it is evident that structure and stoichiometry of sulfur adsorbed on nickel are complex functions of temperature, H_2S concentration, and sulfur coverage, phenomena which account at least in part for the complex nature of nickel poisoning by sulfur. Sulfur poisoning of nickel is most probably a prototype, i.e. similar aspects of complex poisoning behavior are observed in other poison/metal systems, although none have been studied to the same depth as sulfur/nickel.

Since one of the necessary steps in a catalytic reaction is the adsorption of one or more reactants, investigation of the effects of adsorbed sulfur on the adsorption of other molecules, can provide useful insights into the poisoning process [20,26]. Previous investigations [26,36–42] indicate that both H_2 and CO adsorptions on nickel are poisoned by adsorbed sulfur. For example, thermal desorption studies of CO from pre-sulfided Ni(1 0 0) [38] reveal a weakening of the CO adsorption bond and a rapid, non-linear decline in the most strongly bound β_2 state (bridged CO) with increasing sulfur coverage corresponding to a poisoning of about 8–10 Ni atoms for bridged CO adsorption per adsorbed sulfur atom at low sulfur coverage (see Fig. 7); moreover, the β_2-CO species is completely poisoned at about 0.2–0.4 ml of sulfur relative to a saturation coverage of 0.5 ml. Hydrogen adsorption is poisoned in a similar non-linear fashion. On the other hand, the coverage of the β_1 state (linear CO) is constant with increasing sulfur coverage. The sharp non-linear drop in CO and hydrogen adsorptions at low sulfur coverages has been interpreted in terms of a combination of short-range electronic and steric effects operating over a range of less than 5 a.u. [20]. The different effects of sulfur on β_1 and β_2 states of CO have important implications for sulfur poisoning in reactions involving CO; that is, sulfur poisoning can affect reaction selectivity as well as activity [26].

Because sulfur adsorbs so strongly on metals and prevents or modifies the further adsorption of reactant molecules, its presence on a catalyst surface usually effects substantial or complete loss of activity in many important reactions. This is illustrated by the data in Fig. 8 showing the steady-state methanation activities of Ni, Co, Fe, and Ru relative to the fresh, unpoisoned surface activity as a function of gas phase H_2S concentration. These data indicate that Ni, Co, Fe, and Ru all suffer 3–4 orders of magnitude loss in activity at 15–100 ppb of H_2S, i.e. their sulfur tolerances are extremely low! Moreover, the sharp drop in activity with increasing H_2S concentration suggests highly selective poisoning. Nevertheless, the rate of sulfur poisoning and hence sulfur resistance varies from catalyst to catalyst and is apparently a function of catalyst composition [26] and reaction conditions [43]. Indeed, it is possible to significantly improve sulfur resistance of Ni, Co and Fe with catalyst additives such as Mo and B which selectively adsorb sulfur.

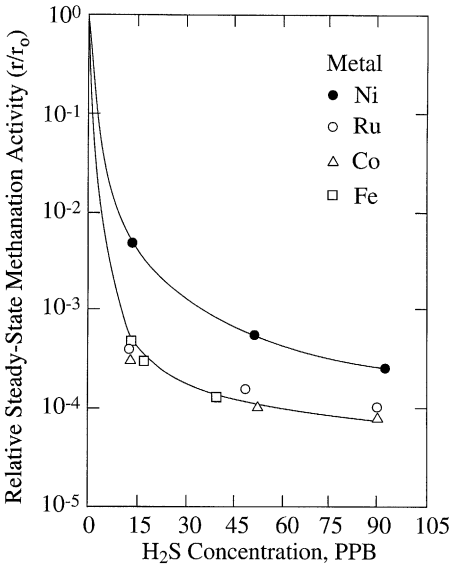

Fig. 8. Relative steady-state methanation activity profiles for Ni (●), Co (△), Fe (□), and Ru (○) as a function of gas phase H_2S concentration. Reaction conditions: 100 kPa; 400°C; 1% CO/99% H_2 for CO, Fe and Ru; 4% CO/96% H_2 for Ni [26].

Because the adsorption of sulfur compounds is generally rapid and irreversible, surface sulfur concentrations in catalyst particles and beds are non-uniform, e.g. H_2S adsorbs selectively at the entrance to a packed bed and on the outer surface of catalyst particles, making the experimental study and modeling of sulfur poisoning (and poisoning by other strongly held poisons) extremely difficult.

There are other complications in the study of sulfur poisoning. For example, the adsorption stoichiometry of sulfur in CO hydrogenation on Ni is apparently a function of the temperature, H_2/CO ratio, and water partial pressure [43]. Moreover, at high CO partial pressures sulfur may be removed from the surface as COS, which is not as strongly adsorbed as H_2S. At low temperature conditions, e.g. those representative of Fischer–Tropsch synthesis or liquid phase hydrogenations, the gas phase concentration of H_2S in poisoning studies must be kept very low, i.e. below 0.1–5 ppm, to avoid formation of bulk metal sulfides — a phenomenon which seriously compromises the validity of the results. Thus, the importance of studying poisoning phenomena in situ under realistic reaction conditions, at low process-relevant poison concentrations, and over a process-representative range of temperature and concentration conditions is emphasized.

There are a number of industrial processes in which one intentionally poisons the catalyst in order to improve its selectivity. For example, Pt-containing naphtha reforming catalysts are often pre-sulfided to minimize unwanted cracking reactions. S and P are added to Ni catalysts to improve isomerization selectivity in the fats and oils hydrogenation industry, while S and Cu are added to Ni catalysts in steam reforming to minimize coking. In catalytic reforming sulfided Re or Sn is added to Pt to enhance the dehydrogenation of paraffins to olefins while poisoning hydrogenolysis/coking reactions. V_2O_5 is added to Pt to suppress SO_2 oxidation to SO_3 in diesel emissions control catalysts.

2.2. Fouling, coking and carbon deposition

Fouling is the physical (mechanical) deposition of species from the fluid phase onto the catalyst surface, which results in activity loss due to blockage of sites and/or pores. In its advanced stages it may result in disintegration of catalyst particles and plugging of the reactor voids. Important examples include mechanical deposits of carbon and coke in porous catalysts, although carbon- and coke-forming processes also involve chemisorption of different kinds of carbons or condensed hydrocarbons which may act as catalyst poisons. The definitions of carbon and coke are somewhat arbitrary and by convention related to their origin. Carbon is typically a product of CO disproportionation while coke is produced by decomposition or condensation of hydrocarbons on catalyst surfaces and typically consists of polymerized heavy hydrocarbons. Nevertheless, coke forms may vary from high molecular weight hydrocarbons to primarily carbons such as graphite, depending upon the conditions under which the coke was formed and aged. A number of books and reviews treat the formation of carbons and coke on catalysts and the attendant deactivation of the catalysts [4,44–49].

The chemical structures of cokes or carbons formed in catalytic processes vary with reaction type, catalyst type, and reaction conditions. Menon [49] has suggested that catalytic reactions accompanied by carbon or coke formation can be broadly classified as either coke-sensitive or coke-insensitive, analogous to

Boudart's more general classification of structure-sensitive and structure-insensitive catalytic reactions. In coke-sensitive reactions, unreactive coke is deposited on active sites leading to activity decline, while in coke-insensitive reactions, relatively reactive coke precursors formed on active sites are readily removed by hydrogen (or other gasifying agents). Examples of coke-sensitive reactions include catalytic cracking and hydrogenolysis; on the other hand, Fischer–Tropsch synthesis, catalytic reforming and methanol synthesis are examples of coke-insensitive reactions. On the basis of this classification Menon [49] reasoned that the structure and location of a coke are more important than its quantity in affecting catalytic activity.

Consistent with Menon's classification, it is also generally observed that not only structure and location of coke vary but also its mechanism of formation varies with catalyst type, e.g. whether it is a metal or metal oxide (or sulfide, sulfides being similar to oxides). Because of these significant differences in mechanism, formation of carbon and coke is discussed below separately for supported metals and for metal oxides and sulfides.

2.2.1. Carbon and coke formation on supported metal catalysts

Possible effects of fouling by carbon (or coke) on the functioning of a supported metal catalyst are illustrated in Fig. 9. Carbon may (1) chemisorb strongly as a monolayer or physically adsorb in multilayers and in either case block access of reactants to metal surface sites, (2) totally encapsulate a metal particle and thereby completely deactivate that particle, and (3) plug micro- and mesopores such that access of reactants is denied to many crystallites inside these pores. Finally, in extreme cases, strong carbon filaments may build-up in pores to the extent that they stress and fracture the support material, ultimately causing disintegration of catalyst pellets and plugging of reactor voids.

Mechanisms of carbon deposition and coke formation on metal catalysts from carbon monoxide and hydrocarbons [4,44–48] are illustrated in Figs. 10 and 11. Different kinds of carbon and coke which vary in morphology and reactivity are formed in these reactions (see Tables 6 and 7). For example, CO dissociates on metals to form Cα, an adsorbed atomic carbon; Cα can react to Cβ, a polymeric carbon

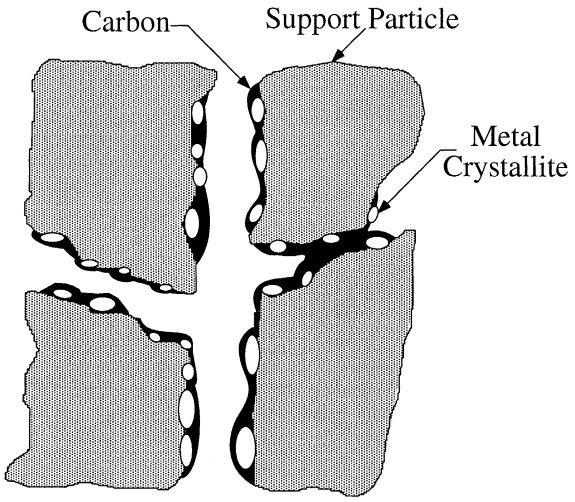

Fig. 9. Conceptual model of fouling, crystallite encapsulation and pore plugging of a supported metal catalyst due to carbon deposition.

film. The more reactive, amorphous forms of carbons formed at low temperatures (e.g. Cα and Cβ) are converted at high temperatures over a period of time to less reactive, graphitic forms [47].

It should also be emphasized, that some forms of carbon result in loss of catalytic activity and some do not. For example, at low temperatures (<300–375°C) condensed polymer or β-carbon films and at high temperatures (>650°C) graphitic carbon films encapsulate the metal surfaces of methanation and steam reforming catalysts [47]. Deactivation of steam reforming catalysts at high reaction temperatures (500–900°C) may be caused by precipitation of atomic (carbidic)

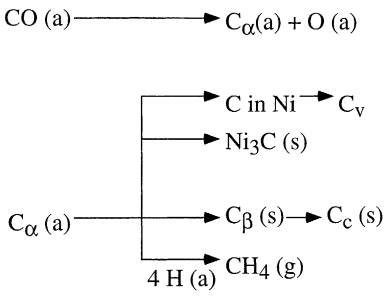

Fig. 10. Formation, transformation and gasification of carbon on nickel (a, g, s refer to adsorbed, gaseous and solid states, respectively) [47].

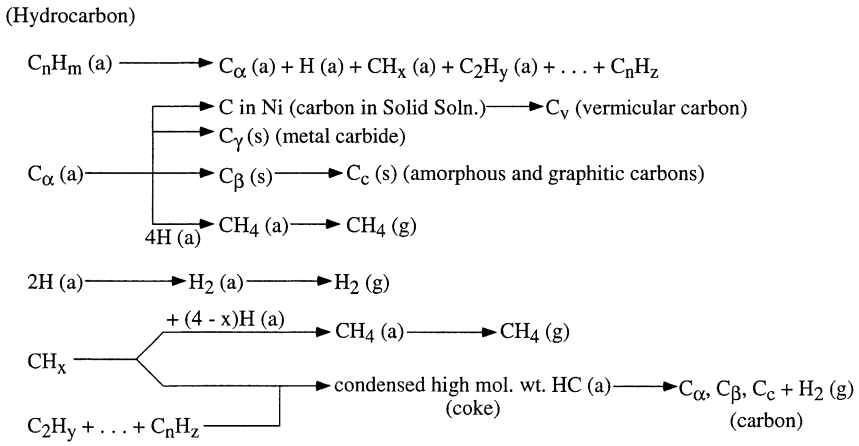

Fig. 11. Formation and transformation of coke on metal surfaces (a, g, s refer to adsorbed, gaseous and solid states, respectively); gas phase reactions are not considered [47].

Table 6
Forms and reactivities of carbon species formed by decomposition of CO on nickel [47]

Structural type	Designation	Temperature of formation (°C)	Peak temperature (°C) for reaction with H_2
Adsorbed, atomic (surface carbide)	C_α	200–400	200
Polymeric, amorphous films or filaments	C_β	250–500	400
Vermicular filaments, fibers, and/or whiskers	C_v	300–1000	400–600
Nickel carbide (bulk)	C_γ	150–250	275
Graphitic (crystalline) platelets or films	C_c	500–550	550–850

carbon dissolved in the Ni-surface layers to a depth of more than 50–70 nm [49,50]. If it accumulates on the metal surface (at high or low temperatures), adsorbed atomic carbon can deactivate metal sites for adsorption and/or reaction. For example, Durer et al. [51] demonstrated that carbon atoms residing in the four-fold hollow sites of Rh(1 0 0) block the adsorption of hydrogen (and hence could block sites for

Table 7
Carbon species formed in steam reforming of hydrocarbons on nickel catalysts [47]

	Encapsulating film	Whisker-like	Pyrolytic carbon
Formation	Slow polymerization of C_nH_m radicals on Ni-surface, into encapsulating film	Diffusion of C through Ni-crystal, nucleation and whisker growth with Ni-crystal at top	Thermal cracking of hydrocarbon; deposition of C precursors on catalyst
Effects	Progressive deactivation	No deactivation of Ni-surface; breakdown of catalyst and increasing ΔP	Encapsulation of catalyst particle; deactivation and increasing ΔP
Temperature range (°C)	<500	>450	>600
Critical parameters	Low temperature Low H_2O/C_nH_m Low H_2/C_nH_m Aromatic feed	High temperature Low H_2O/C_nH_m No enhanced H_2O adsorption Low activity Aromatic feed	High temperature High void fraction Low H_2O/C_nH_m High pressure Acidic catalyst

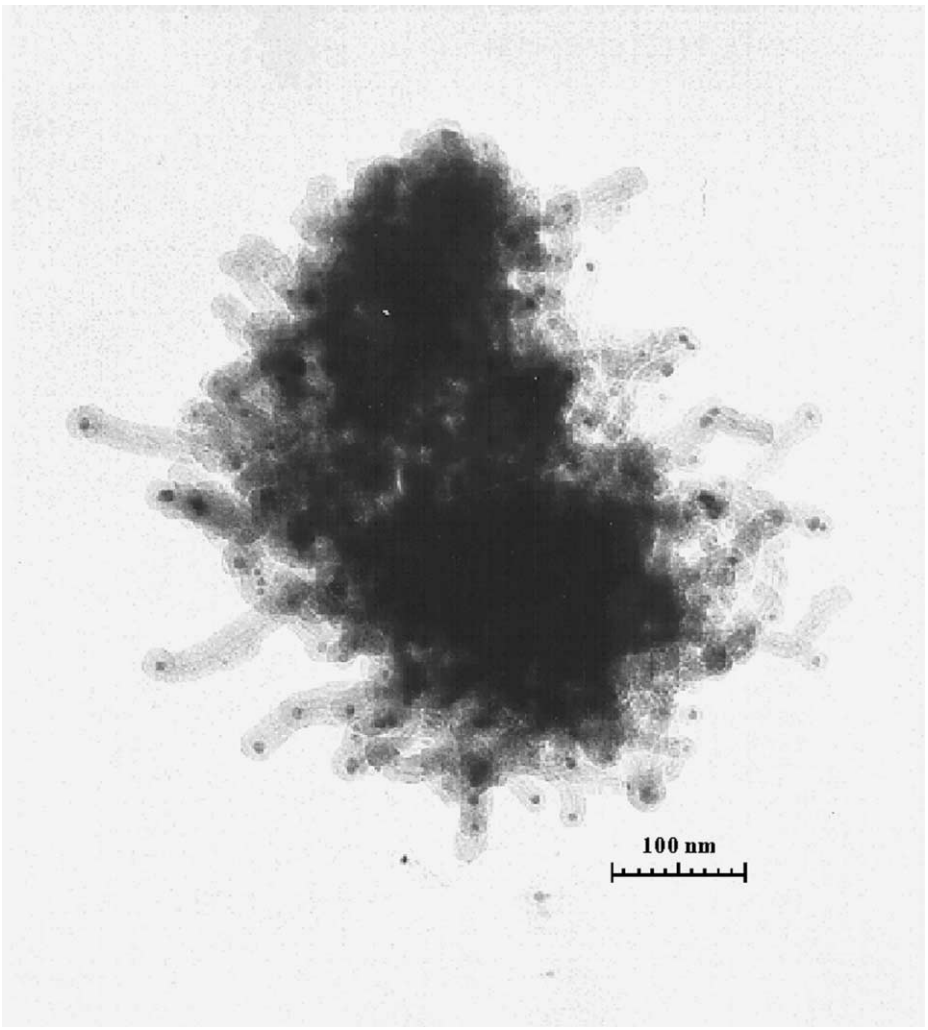

Fig. 12. Electron micrograph of 14% Ni/Al_2O_3 having undergone extensive carbon deposition during CO disproportionation at 673 K, $P_{CO} = 4.55$ kPa (magnification of 200,000; courtesy: BYU Catalysis Laboratory).

hydrogenation). In the intermediate temperature range of 375–650°C, carbon filaments (Fig. 12) are formed by precipitation of dissolved carbon at the rear side of metal crystallites causing the metal particles to grow away from the support [44]. Filament growth ceases when sufficient carbon accumulates on the free surface to cause encapsulation by a carbon layer; however, encapsulation of the metal particles does not occur if H_2/CO or H_2O/hydrocarbon ratios are sufficiently high. Thus, carbon filaments sometimes formed in CO hydrogenation or steam reforming of hydrocarbons would not necessarily cause a loss of intrinsic catalyst activity unless they are formed in sufficient quantities to cause plugging of the pores [47] or loss of metal occurs as the carbon fibers are removed during regeneration [52,53]. However, in practice, regions of carbon forming potential in steam reforming must be carefully avoided, since once initiated, the rates of filamentous carbon formation are sufficiently high to cause catastrophic pore plugging and catalyst failure within a few hours to days.

The rate at which deactivation occurs for a given catalyst and reaction depends greatly on reaction

conditions — especially temperature and reactant composition. A fundamental principle for coke-insensitive reactions on metals (e.g. methanation, Fischer–Tropsch synthesis, steam-reforming, catalytic reforming and methanol synthesis) is that deactivation rate depends greatly on the difference in rates of formation and gasification of carbon/coke precursors, i.e. $r_d = r_f - r_g$. If the rate of gasification r_g is equal to or greater than that of formation r_f carbon/coke is not deposited. Rates of carbon/coke precursor formation and gasification both increase exponentially with temperature, although the difference between them varies a great deal with temperature because of differences in pre-exponential factors and activation energies. Thus, carbon/coke formation is avoided in regions of temperature in which precursor gasification rate exceeds deposition rate. This is illustrated in Fig. 13, an Arrhenius plot for rates of formation and hydrogenation of alpha and beta carbons on nickel during CO methanation. Since at temperatures below 600 K ($1/T > 1.66 \times 10^{-3}\ K^{-1}$) the rate of C_α gasification exceeds that of C_α formation, no carbon is deposited. However above 600 K, C_α accumulates on the surface since the rate of C_α formation exceeds that of C_α gasification. As C_α accumulates (at 600–700 K), it is converted to a C_β polymeric chain or film which deactivates the nickel catalyst; however, above 700 K ($1/T < 1.43 \times 10^{-3}\ K^{-1}$) the rate of C_β hydrogenation exceeds that of formation and no deactivation occurs. Thus, the "safe" regions of methanation for avoiding deactivation by carbon are below 600 and above 700 K; of course, these regions will vary somewhat with reactant concentrations and catalyst activity. A similar principle operates in steam reforming, i.e. at a sufficiently low reaction temperature, the rate of hydrocarbon adsorption exceeds the rate of hydrocracking and a deactivating polymer film is formed [54]; accordingly, it is necessary to operate above this temperature to avoid deactivation.

In steam reforming filamentous carbon formation rate is a strong function of hydrocarbon structure; for example, it decreases in the order acetylenes, olefins, paraffins, i.e. in the order of decreasing reactivity, although activation energies for nickel are in the same range (125–139 kJ) independent of hydrocarbon structure and about the same as those observed for formation of filamentous carbon from decomposition of CO [47]. This latter observation suggests that the reactions of CO and different hydrocarbons to filamentous carbon proceed by a common mechanism and rate

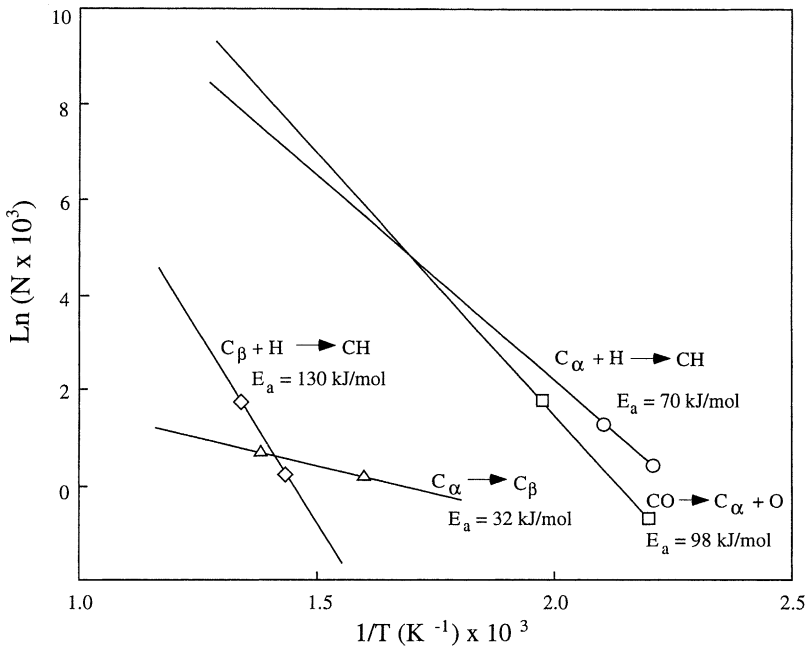

Fig. 13. Rates of formation (ln scale) and hydrogenation of C_α and C_β vs. reciprocal temperature [47].

determining step — probably the diffusion of carbon through the metal crystallites [47].

The rate at which a carbon or coke is accumulated in a given reaction under given conditions can vary significantly with catalyst structure, including metal type, metal crystallite size, promoter, and catalyst support. For example, supported Co, Fe and Ni are active above 350–400°C for filamentous carbon formation from CO and hydrocarbons; the order of decreasing activity is reportedly Fe, Co, and Ni [47]. Pt, Ru and Rh catalysts, on the other hand, while equally or more active than Ni, Co, or Fe in steam reforming produce little or no coke or carbon. This is attributed to reduced mobility and/or solubility of carbon in the noble metals, thus retarding the nucleation process. Thus, it is not surprising that addition of noble metals to base metals retards carbon formation; for example, addition of Pt in Ni lowers carbon deposition rate during methanation, while addition of Cu to Ni substantially lowers carbon formation in steam reforming [47]. In a detailed surface science study of submonolayers of Au on Ni(1 1 1), Besenbacher et al. [55] found using STM that the electron density of Ni atoms in the vicinity of Au atoms was increased and from DFT calculations that the strength of carbon adsorption (and hence the tendency to form graphite) was decreased on next-nearest neighbor Ni atoms; from studies of the effects of S adsorption on methane activation and graphite formation on pure Ni, they were able to infer that the ensemble size needed for methane dissociation is smaller than that for graphite formation. These fundamental insights were used in the design of an industrial 0.3% Au-promoted 16% $Ni/MgAl_2O_4$ catalyst which loses no activity over 4000 h during steam reforming of *n*-butane, while the corresponding unpromoted Ni catalyst loses about 5% of its initial activity. In contrast to the moderating effects of noble metal additives, addition of 0.5% Sn to cobalt substantially increases the rate of carbon filament formation from ethylene [56], an effect desirable in the commercial production of carbon filament fibers.

Since carbon formation and gasification rates are influenced differently by modifications in metal crystallite surface chemistry which are in turn a function of catalyst structure; oxide additives or oxide supports may be used to moderate the rate of undesirable carbon or coke accumulation. For example, Bartholomew et al. [57] found the specific rate (turnover frequency) of filamentous carbon deposition on nickel during methanation at 350°C to decrease in the order Ni/TiO_2, $NiAl_2O_3$, Ni/SiO_2, while Vance and Bartholomew [58] observed C_α hydrogenation rates at 170°C to decrease in this same order (the same as for methanation at 225°C). This behavior was explained in terms of promotional or inhibiting effects due to decoration of metal crystallites by the support, silica, for example, inhibiting both CO dissociation and carbon hydrogenation. This hypothesis is consistent with observations [59,60] that silica evaporated on metal surfaces and supported metals inhibits formation of filamentous carbon. Similarly Bitter et al. [61] observed rates of carbon formation in CO_2/CH_4 reforming to decrease in the order $Pt/\gamma\text{-}Al_2O_3 \gg Pt/TiO_2 > Pt/ZrO_2$; while 90% of the carbon deposited on the support, the authors linked deactivation to carbon accumulated on the metal due to an imbalance between carbon formed by methane dissociation and oxidation by chemisorbed CO_2. The rate of formation of coke in steam reforming is delayed and occurs at lower rates in nickel catalysts promoted with alkali or supported on basic MgO [62].

Since formation of coke, graphite or filamentous carbon involves the formation of C–C bonds on multiple atoms sites, one might expect that coke or carbon formation on metals is structure-sensitive, i.e. sensitive to surface structure and metal crystallite size. Indeed, Bitter et al. [61] found that catalysts containing larger Pt crystallites deactivate more rapidly during CO_2/CH_4 reforming than those containing small crystallites. However, a crystallite size effect, observed in steam reforming of methane on nickel [47,62], appears to operate in the opposite direction, i.e. formation of filamentous carbon occurs at higher rates in catalysts containing smaller metal crystallites.

In summary, deactivation of supported metals by carbon or coke may occur chemically due to chemisorption or carbide formation or physically due to blocking of surface sites, metal crystallite encapsulation, plugging of pores, and destruction of catalyst pellets by carbon filaments. Blocking of catalytic sites by chemisorbed hydrocarbons, surface carbides or relatively reactive films is generally reversible in hydrogen, steam, CO_2 or oxygen. Further details of the thermodynamics, kinetics, and mechanisms of carbon and coke formation in methanation and steam reforming reactions are available in reviews by Bartholomew [47] and Rostrup-Nielsen [54,62].

2.2.2. Coke formation on metal oxide and sulfide catalysts

In reactions involving hydrocarbons, coke may be formed in the gas phase and on both non-catalytic and catalytic surfaces. Nevertheless, formation of coke on oxides and sulfides is principally a result of cracking reactions involving coke precursors (typically olefins or aromatics) catalyzed by acid sites [63,64]. Dehydrogenation and cyclization reactions of carbocation intermediates formed on acid sites lead to aromatics which react further to higher molecular weight polynuclear aromatics and condense as coke (see Fig. 14).

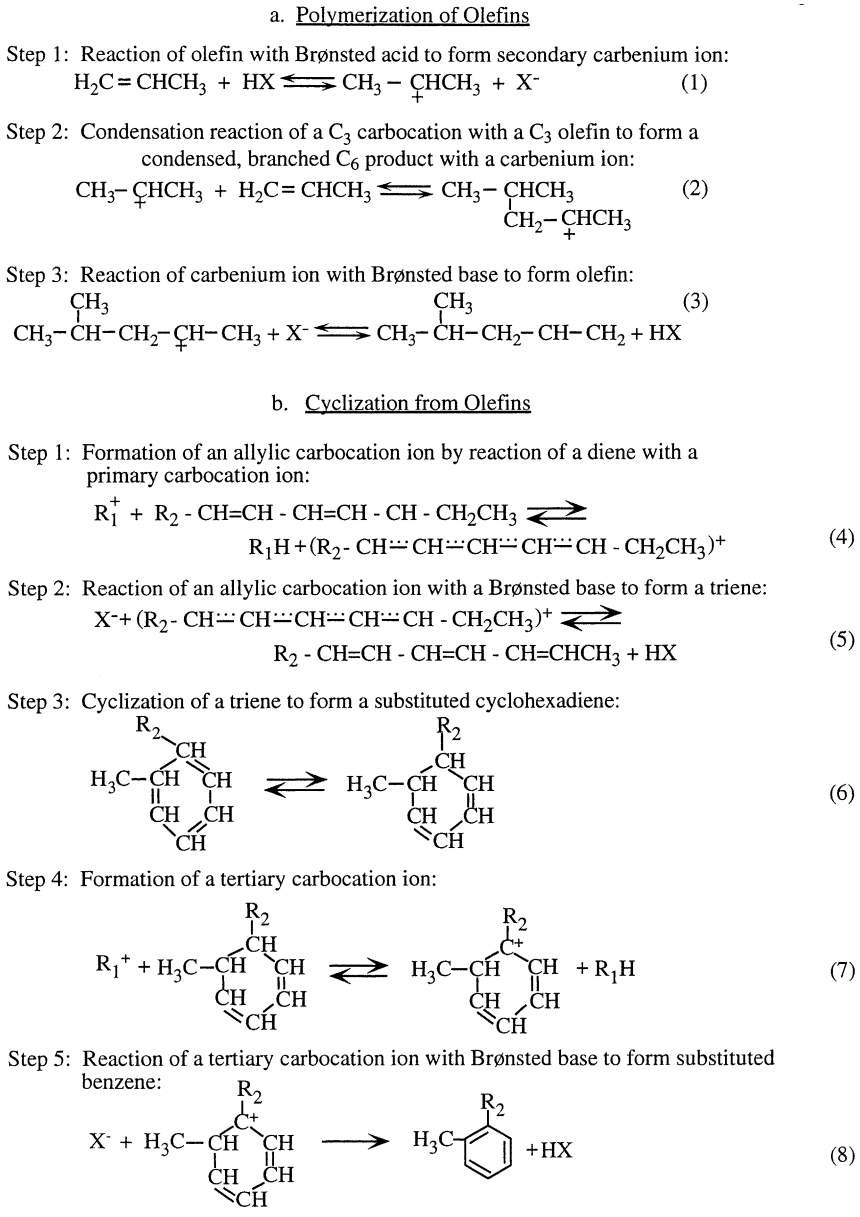

Fig. 14. Coke-forming reactions of alkenes and aromatics on oxide and sulfide catalysts: (a) polymerization of alkenes; (b) cyclization from alkenes; (c) formation of polynuclear aromatics from benzene ([8]; courtesy: Kluwer Academic Publishers).

c. Formation of Polynuclear Aromatics from Benzene

Step 1: Initiation (protonation of benzene):

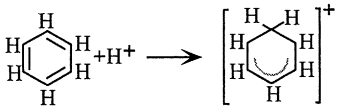

(9)

Step 2: Propagation (condensation reaction of carbocation with benzene followed by H abstraction):

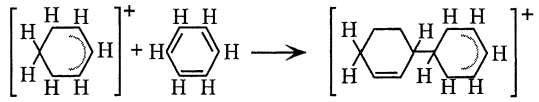

(10)

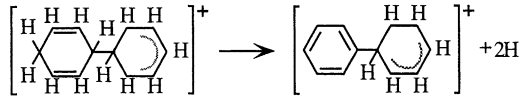

(11)

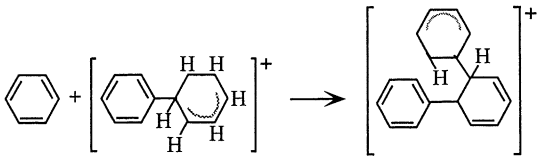

(12)

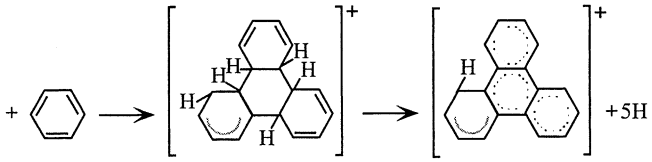

(13)

and so forth.

Step 3: Termination (reaction of carbocation with Brønsted base):

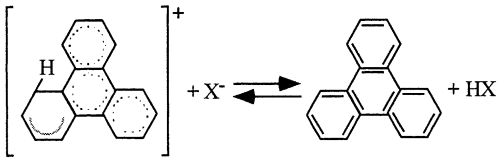

(14)

Fig. 14 (*Continued*).

Reactions 1–3 in Fig. 14 illustrate the polymerization of olefins, reactions 4–8 illustrate cyclization from olefins, and reactions 9–14 illustrate chain reaction formation of polynuclear aromatics which condense as coke on the catalyst surface. Because of the high stability of the polynuclear carbocations (formed in reactions 10–13), they can continue to grow on the surface for a relatively long time before a termination reaction occurs through the back donation of a proton.

From this mechanistic scheme (Fig. 14) it is clear that olefins, benzene and benzene derivatives, and polynuclear aromatics are precursors to coke formation. However, the order of reactivity for coke formation is clearly structure dependent, i.e. polynuclear aromatics > aromatics > olefins > branched alkanes > normal alkanes. For example, the amount of coke formed on silica/alumina at 500°C is 0.06, 3.8, 12.5, and 23 wt.% for benzene, naphthalene, fluoranthene, and anthracene, respectively [65].

Coking reactions in processes involving heavy hydrocarbons are very complex; different kinds of coke may be formed and cokes may range in composition from CH to C and have a wide range of reactivities with oxygen and hydrogen depending upon the time-on-stream and temperature to which they are exposed. For example, coke deposits occurring in hydrodesulfurization of residue have been classified into three types [66]:

1. Type I deposits are reversibly adsorbed normal aromatics deposited during the first part of the cycle at low temperature.
2. Type II deposits are reversibly adsorbed asphaltenes deposited early in the coking process.
3. Type III deposits result from condensation of aromatic concentrates into clusters and then crystals which constitute a "mesophase". This crystalline phase is formed after long reaction times at high temperature. This hardened coke causes severe deactivation of the catalyst [66].

In addition to hydrocarbon structure and reaction conditions, extent and rate of coke formation are also a function of the acidity and pore structure of the catalyst. Generally, the rate and extent of coke formation increase with increasing acid strength and concentration. Coke yield decreases with decreasing pore size (for a fixed acid strength and concentration); this is especially true in zeolites where shape selectivity plays an important role in coke formation. For example, coke yield in fluid catalytic cracking is only 0.4% for ZSM-5 (pore diameters of 0.54 mm × 0.56 nm) compared to 2.2% for Y-faujasite (aperture diameter of 0.72 nm) [64]. However, in pores of molecular diameter, a relatively small quantity of coke can cause substantial loss of activity. It should be emphasized that coke yield can vary considerably into the interior pores of a catalyst particle or along a catalyst bed depending upon the extent to which the main and deactivation reactions are affected by film mass transport and pore diffusional resistance.

The mechanisms by which coke deactivates oxide and sulfide catalysts are, as in the case of supported metals, both chemical and physical. However, some aspects of the chemistry are quite different. The principle chemical loss of activity in oxides and sulfides is due to the strong adsorption of coke molecules on acidic sites. But as discussed earlier, strong acid sites also play an important role in the formation of coke precursors which subsequently undergo condensation reactions to produce large polynuclear aromatic molecules that physically coat catalytic surfaces. Physical loss of activity also occurs as coke accumulates, ultimately partially or completely blocking catalyst pores as in supported metal catalysts. For example, in isomerization of *cis*-butene on SiO_2/Al_2O_3 [67] catalyst deactivation occurs by rapid, selective poisoning of strong acid sites; coke evolved early in the reaction is soluble in dichloromethane and pyridine and is slightly aromatic. Apparently, the blocking of active sites does not significantly affect porosity or catalyst surface area, as SiO_2/Al_2O_3 contains relatively large mesopores.

In the case of supported bifunctional metal/metal oxide catalysts, different kinds of coke are formed on the metal and the acidic oxide support, e.g. soft coke (high H/C ratio) on Pt or Pt-Re metals and hard coke (low H/C ratio) on the alumina support in catalytic reforming [68]. In this case, coke precursors may be formed on the metal via hydrogenolysis, following which they migrate to the support and undergo polymerization and cyclization reactions, after which the larger molecules are dehydrogenated on the metal and finally accumulate on the support causing loss of isomerization activity. Mild sulfiding of these catalysts (especially Pt-Re/alumina) substantially reduces the rate of hydrogenolysis and the overall formation of coke on both metal and support; it especially reduces the hard coke, which is mainly responsible for deactivation.

Several recent studies [64,69–79] have focused on coke formation during hydrocarbon reactions in zeolites including (1) the detailed chemistry of coke precursors and coke molecules formed in zeolite pores and pore intersections (or supercages) and (2) the relative importance of adsorption on acid sites versus pore blockage. The principal conclusions from these studies can be summarized as follows: (1) the formation of coke and the manner in which it deactivates a zeolite catalyst are shape-selective processes, (2) deactivation is mainly due to the formation and retention of heavy aromatic clusters in pores and pore intersections, and (3) while both acid-site poisoning and pore blockage participate in the deactivation, the former dominates at low coking rates, low coke coverages (e.g. in Y-zeolite below 2 wt.%) and high temperatures,

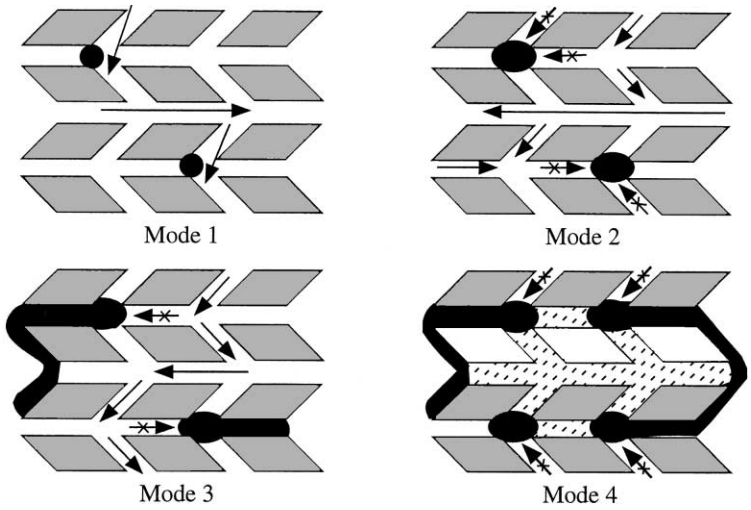

Fig. 15. Schematic of the four possible modes of deactivation by carbonaceous deposits in HZSM-5: (1) reversible adsorption on acid sites, (2) irreversible adsorption on sites with partial blocking of pore intersections, (3) partial steric blocking of pores, and (4) extensive steric blocking of pores by exterior deposits [77].

while the latter process dominates at high reaction rates, low temperatures, and high coke coverages. Thus, pore size and pore structure are probably more important than acid strength and density under typical commercial process conditions. Indeed, deactivation is typically more rapid in zeolites having small pores or apertures and/or a monodimensional structure [77]. Fig. 15 illustrates four possible modes of deactivation of HZSM-5 by carbonaceous deposits with increasing severity of coking according to Guisnet et al. [77].

These conclusions (in the previous paragraph) are borne out, for example, in the study by Cerqueira et al. [79] of USHY-zeolite deactivation during methylcyclohexane transformation at 450°C showing the following:

1. Coke is probably mainly formed by rapid transformation of ethylenic C_7 carbenium ions with lesser contributions from reactions of cyclopentadiene, C_3–C_6 olefins, and aromatics.
2. Soluble coke consists of polynuclear aromatic clusters containing three to seven five- and six-membered rings having a typical compositions of $C_{30}H_{40}$ to $C_{40}H_{44}$ and having dimensions of 0.9 mm × 1.1 nm to 1.1 mm × 1.5 nm, i.e. sizes that would cause them to be trapped in the supercages of Y-zeolite.
3. At short contact times, coking is relatively slow and deactivation is mainly due to acid-site poisoning, while at long contact times, coking is much faster because of the high concentrations of coke precursors; under these latter conditions coke is preferentially deposited at the outer pore openings of zeolite crystallites and deactivation is dominated by pore mouth blockage.

That coke formed at large contact times not only blocks pores and/or pore intersections inside the zeolite, but also migrates to the outside of zeolite crystallites where it blocks pore entrances has been observed in several studies [73,75,76,79]. However, the amount, structure and location of coke in ZSM-5 depends strongly on the coke precursor, e.g. coke formed from mesitylene is deposited on the external zeolite surface, whereas coking with isobutene leads to largely paraffinic deposits inside pores; coke from toluene, on the other hand, is polyaromatic and is deposited both on external and internal zeolite surfaces [73].

2.3. Thermal degradation and sintering

2.3.1. Background

Thermally induced deactivation of catalysts results from (i) loss of catalytic surface area due to crystallite

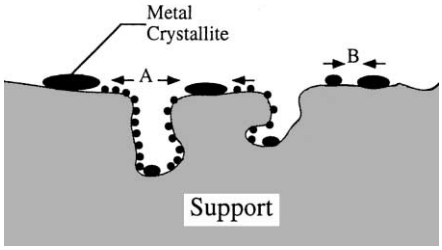

Fig. 16. Two conceptual models for crystallite growth due to sintering by (A) atomic migration or (B) crystallite migration.

growth of the catalytic phase, (ii) loss of support area due to support collapse and of catalytic surface area due to pore collapse on crystallites of the active phase, and/or (iii) chemical transformations of catalytic phases to non-catalytic phases. The first two processes are typically referred to as "sintering". The third is discussed in the next section under solid–solid reactions. Sintering processes generally take place at high reaction temperatures (e.g. >500°C) and are generally accelerated by the presence of water vapor.

Most of the previous sintering and redispersion work has focused on supported metals. Experimental and theoretical studies of sintering and redispersion of supported metals published before 1997 have been reviewed fairly extensively [8,80–89]. Three principal mechanisms of metal crystallite growth have been advanced: (1) crystallite migration, (2) atomic migration, and (3) (at very high temperatures) vapor transport. The processes of crystallite and atomic migration are illustrated in Fig. 16. Crystallite migration involves the migration of entire crystallites over the support surface followed by collision and coalescence. Atomic migration involves detachment of metal atoms from crystallites, migration of these atoms over the support surface and ultimately, capture by larger crystallites. Redispersion, the reverse of crystallite growth in the presence of O_2 and/or Cl_2, may involve (1) formation of volatile metal oxide or metal chloride complexes which attach to the support and are subsequently decomposed to small crystallites upon reduction and/or (2) formation of oxide particles or films that break into small crystallites during subsequent reduction.

There has been some controversy in the literature regarding which mechanism of sintering (or redispersion) operates at a given set of conditions. However, each of the three sintering mechanisms (and two dispersion mechanisms) is a simplification which ignores the possibility that all mechanisms may occur simultaneously and may be coupled with each other through complex physicochemical processes including the following: (1) dissociation and emission of metal atoms or metal-containing molecules from metal crystallites, (2) adsorption and trapping of metal atoms or metal-containing molecules on the support surface, (3) diffusion of metal atoms, metal-containing molecules and/or metal crystallites across support surfaces, (4) metal or metal oxide particle spreading, (5) support surface wetting by metal or metal oxide particles, (6) metal particle nucleation, (7) coalescence of, or bridging between, two metal particles, (8) capture of atoms or molecules by metal particles, (9) liquid formation, (10) metal volatilization through volatile compound formation, (11) splitting of crystallites in O_2 atmosphere due to formation of oxides of a different specific volume, and (12) metal atom vaporization. Depending upon reaction or redispersion conditions, a few or all of these processes may be important; thus, the complexity of sintering/redispersion processes is emphasized.

In general, sintering processes are kinetically slow (at moderate reaction temperatures) and irreversible or difficult to reverse. Thus, sintering is more easily prevented than cured.

2.3.2. Factors affecting metal particle growth and redispersion in supported metals

Temperature, atmosphere, metal type, metal dispersion, promoters/impurities and support surface area, texture and porosity, are the principal parameters affecting rates of sintering and redispersion (see Table 8, [8,85–89]). Sintering rates increase exponentially with temperature. Metals sinter relatively rapidly in oxygen and relatively slowly in hydrogen, although depending upon the support, metal redispersion can be facilitated by exposure at high temperature (e.g. 500–550°C for Pt/Al_2O_3) to oxygen and chlorine followed by reduction. Water vapor also increases the sintering rate of supported metals.

Normalized dispersion (percentage of metal exposed at any time divided by the initial percentage exposed) versus time data in Fig. 17 show that at temperatures of 650°C or higher, rates of metal surface area loss (measured by hydrogen chemisorption) due to sintering of Ni/silica in hydrogen atmosphere

Table 8
Effects of important reaction and catalyst variables on sintering rates of supported metals based on GPLE data [8,85–89]

Variable	Effect
Temperature	Sintering rates are exponentially dependent on T; E_{act} varies from 30 to 150 kJ/mol; E_{act} decreases with increasing metal loading; it increases in the following order with atmosphere: NO, O_2, H_2, N_2
Atmosphere	Sintering rates are much higher for noble metals in O_2 than in H_2 and higher for noble and base metals in H_2 relative to N_2; sintering rate decreases for supported Pt in atmospheres in the following order: NO, O_2, H_2, N_2
Metal	Observed order of decreasing thermal stability in H_2 is Ru > Ir ≅ Rh > Pt; thermal stability in O_2 is a function of (1) volatility of metal oxide and (2) strength of metal oxide–support interaction
Support	Metal–support interactions are weak (bond strengths of 5–15 kJ/mol); with a few exceptions, thermal stability for a given metal decreases with support in the following order: Al_2O_3 > SiO_2 > carbon
Promoters	Some additives decrease atom mobility, e.g. C, O, CaO, BaO, CeO_2, GeO_2; others increase atom mobility, e.g. Pb, Bi, Cl, F, or S; oxides of Ba, Ca, or Sr are "trapping agents" that decrease sintering rate
Pore size	Sintering rates are lower for porous vs. non-porous supports; they decrease as crystallite diameters approach those of the pores

are significant, causing 70% loss of the original metal surface area within 50 h at 750°C. In reducing atmosphere, metal crystallite stability generally decreases with decreasing metal melting temperature, i.e. in the order Ru > Ir > Rh > Pt > Pd > Ni > Cu > Ag, although this order may be affected by relatively stronger metal–support interactions, e.g. the observed order of decreasing stability of supported platinum in vacuum is Pt/Al_2O_3 > Pt/SiO_2 > Pt/C. In oxidizing atmospheres, metal crystallite stability depends on the volatility of metal oxides and the strength of the metal oxide–support interaction. For noble metals, metal stability in air decreases in the order Rh > Pt > Ir > Ru; formation of volatile RuO_4 accounts for the relative instability of ruthenium.

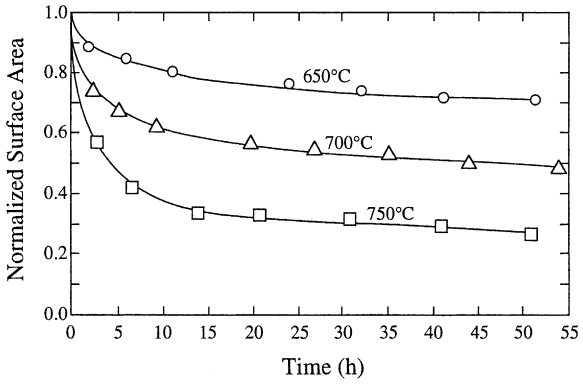

Fig. 17. Normalized nickel surface area (based on H_2 adsorption) vs. time data during sintering of 13.5% Ni/SiO_2 in H_2 at 650, 700 and 750°C [93].

Promoters or impurities affect sintering and redispersion by either increasing (e.g. chlorine and sulfur) or decreasing (e.g. oxygen, calcium and cesium) metal atom mobility on the support. Similarly, support surface defects or pores impede surface migration of metal particles — especially micropores and mesopores with pore diameters about the same size as the metal crystallite.

Historically, sintering rate data were fitted to a simple power law expression (SPLE) of the form:

$$-\frac{\mathrm{d}(D/D_0)}{\mathrm{d}t} = k_s \left(\frac{D}{D_0}\right)^n \quad (1)$$

where k_s is the sintering rate constant, D_0 the initial dispersion, and n is the sintering order, which for typical catalyst systems may vary from 3 to 15; unfortunately, the SPLE is in general not valid for sintering processes because it assumes that surface area or dispersion ultimately reaches zero given sufficient time, when in fact, for a given temperature and atmosphere, a non-zero or limiting dispersion is observed after long sintering times. Moreover, the use of the SPLE is further questionable because variations in sintering order are observed as a function of time and temperature for a given catalyst in a fixed atmosphere [87–89]; thus, data obtained for different samples and different reaction conditions cannot be quantitatively compared. Nevertheless, it has been shown by Fuentes [90] and Bartholomew and co-workers [85–88] that the effects of temperature, atmosphere, metal, promoter, and support can be quantitatively determined

Table 9
Comparison of second-order sintering rate constants and activation energies for Pt, Ni and Ag catalysts [88]

Catalyst	Atmosphere	D_0[a]	k_s[b] (400°C)	k_s (650°C)	k_s (700°C)	k_s (750°C)	E_{act}[c] (kJ/mol)	Reference
0.6% Pt/γ-Al_2O_3	H_2	~0.85	0.007	0.310	0.530	1.32	79	[91]
5% Pt/Al_2O_3	H_2	0.10	0.420	0.76	0.84	0.97	13	[92]
15% Ni/γ-Al_2O_3	H_2	0.16	0.004	0.083	0.13	0.27	66	[93]
0.6% Pt/γ-Al_2O_3	Air	~0.85	0.024	0.29	0.41	0.75	52	[91]
5% Pt/Al_2O_3	Air	0.10	0.014	1.46	2.79	8.51	97	[92]
1.8% Ag/η-Al_2O_3	Air	0.36	0.69					[94]

[a] Initial metal dispersion or percentage exposed.
[b] Second-order sintering rate constant from general power law expression (GPLE) with units of h^{-1}.
[c] Sintering activation energy for GPLE: $-d(D/D_0)/dt = k_s[D/D_0 - D_{eq}/D_0]^m$, where $m = 2$.

by fitting sintering kinetic data to the general power law expression (GPLE)

$$-\frac{d(D/D_0)}{dt} = k_s\left(\frac{D}{D_0} - \frac{D_{eq}}{D_0}\right)^m \quad (2)$$

which adds a term $-D_{eq}/D_0$ to account for the observed asymptotic approach of the typical dispersion versus time curve to a limiting dispersion D_{eq} at infinite time; m, the order of sintering, is found to be either 1 or 2. A recently compiled, comprehensive quantitative treatment of previous sintering rate data based on the GPLE with an order of 2 ($m = 2$) [86–88] quantitatively addresses the effects of catalyst properties and reaction conditions on sintering rate. Some of these data are summarized in Table 9 [91–94]. These data show, for example, that the rate constant and hence the rate of sintering is less for Ni/alumina than for Pt/alumina, an unexpected result in view of the lower heat of vaporization for Ni. This result is possibly explained by a greater metal–support interaction for Ni with alumina.

Sintering studies of supported metals are generally of two types: (1) studies of commercially-relevant supported metal catalysts, and (2) studies of model metal–support systems. The former type provides useful rate data that can be used to predict sintering rates, while the latter type provides insights into the mechanisms of metal particle migration and sintering, although the results cannot be quantitatively extrapolated to predict behavior of commercial catalysts. There is direct evidence from the previous studies of model-supported catalysts [86,89] for the occurrence of crystallite migration (mainly in well-dispersed systems early in the sintering process), atomic migration (mainly at longer sintering times) and spreading of metal crystallites (mainly in oxygen atmosphere). There is also evidence that under reaction conditions, the surface is dynamic, i.e. adsorbates and other adatoms rapidly restructure the surface and slowly bring about faceting; moreover, thermal treatments cause gradual changes in the distribution of coordination sites to minimize surface energy. There is a trend in increasing sophistication of spectroscopic tools used to study sintering and redispersion. In the next decade we might expect additional insights into atomic and molecular processes during reaction at the atomic scale using STM, analytical HRTEM, and other such powerful surface science tools.

2.3.3. Sintering of catalyst carriers

Sintering of carriers has been reviewed by Baker et al. [85] and Trimm [95]. Single phase oxide carriers sinter by one or more of the following processes: (1) surface diffusion, (2) solid-state diffusion, (3) evaporation/condensation of volatile atoms or molecules, (4) grain boundary diffusion, and (5) phase transformations. In oxidizing atmospheres, γ-alumina and silica are the most thermally stable carriers; in reducing atmospheres, carbons are the most thermally stable carriers. Additives and impurities affect the thermal properties of carriers by occupying defect sites or forming new phases. Alkali metals, for example, accelerate sintering; while calcium, barium, nickel, and lanthanum oxides form thermally stable spinel phases with alumina. Steam accelerates support sintering by forming mobile surface hydroxyl groups that are subsequently volatilized at higher temperatures. Chlorine also promotes sintering and grain growth in magnesia and titania during high temperature calcination. This is illustrated in Fig. 18

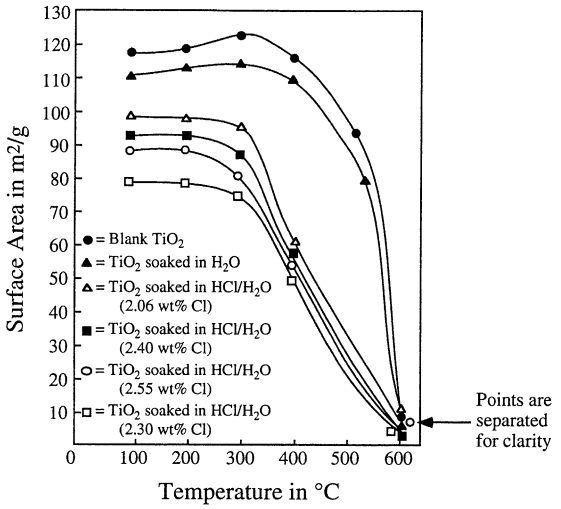

Fig. 18. BET surface area of titania as a function of thermal treatment and chlorine content of fresh samples (before pretreatment). Samples were treated at the temperature indicated for 2 h [96].

[96]. By contrast, sulfuric acid treatment of hydrated alumina (gibbsite) followed by two-step calcination, results in a very stable transitional alumina with needle-like particle morphology [95]. Dispersed metals in supported metal catalysts can also accelerate support sintering, for example, dispersed nickel accelerates the loss of Al_2O_3 surface area in Ni/Al_2O_3 catalysts.

2.3.4. Effects of sintering on catalyst activity

Baker et al. [85] have reviewed the effects of sintering on catalytic activity. Specific activity (based on catalytic surface area) can either increase or decrease with increasing metal crystallite size during sintering if the reaction is structure-sensitive, or it can be independent of changes in metal crystallite size if the reaction is structure-insensitive. Thus, for a structure-sensitive reaction, the impact of sintering may be either magnified or moderated; while for a structure insensitive-reaction, sintering has in principle no effect on specific activity (per unit surface area). In the latter case, the decrease in mass-based activity is proportional to the decrease in metal surface area. Ethane hydrogenolysis and ethane steam reforming are examples of structure-sensitive reactions, while CO hydrogenation on supported cobalt, nickel, iron and ruthenium is structure-insensitive.

2.3.5. Mechanisms and models of sintering and redispersion

There are a number of different models of sintering and redispersion [85] which can be classified as empirical, phenomenological, probabilistic, and mechanistic. The GPLE is an empirical model. The most common phenomenological models are ripening models (involving atom migration), coagulation models (involving crystallite migration) and interfacial thermodynamic models (involving spreading and splitting of crystallites). Probabilistic models include statistical and molecular dynamics models. Mechanistic models are detailed chemical models. The existing models for sintering and redispersion do not simulate observed phenomena over sufficiently wide ranges of conditions. More general models are needed to simulate the complex, simultaneous processes that occur during sintering and redispersion. With the advent of relatively inexpensive, powerful, high-speed computers, the application of molecular dynamics and other mechanistic models of sintering and redispersion processes portends great promise for achieving more realistic simulations.

2.4. Gas/vapor–solid and solid-state reactions

In addition to poisoning, there are a number of chemical routes leading to catalyst deactivation: (1) reactions of the vapor phase with the catalyst surface to produce (a) inactive bulk and surface phases (rather than strongly adsorbed species) or (b) volatile compounds which exit the catalyst and reactor in the vapor phase, (2) catalytic solid–support or catalytic solid–promoter reactions, and (3) solid-state transformations of the catalytic phases during reaction. Each of these routes is discussed in some detail below.

2.4.1. Gas/vapor–solid reactions

2.4.1.1. Reactions of gas/vapor with solid to produce inactive phases. Dispersed metals, metal oxides, metal sulfides, and metal carbides are typical catalytic phases, the surfaces of which are similar in composition to the bulk phases. For a given reaction, one of these catalyst types is generally substantially more active than the others, e.g. only Fe and Ru metals are active for ammonia synthesis, while the oxides, sulfides, and carbides are inactive. If, therefore, one of

Table 10
Examples of reactions of gases/vapors with catalytic solids to produce inactive phases

Catalytic process	Gas/vapor composition	Catalytic solid	Deactivating chemical reaction	References
Auto emissions control	N_2, O_2, HCs, CO, NO	Pt-Rh/Al_2O_3	$2Rh_2O_3 + \gamma\text{-}Al_2O_3 \rightarrow RhAl_2O_4 + 0.5O_2$	[97,98]
Ammonia synthesis and regeneration	H_2, N_2 Traces O_2, H_2O	Fe/K/Al_2O_3	Fe → FeO at >50 ppm O_2 Fe → FeO at $H_2O/H_2 > 0.16$	[8]
Catalytic cracking	HCs, H_2, H_2O	LaY-zeolite	H_2O induced Al migration from zeolite framework causing zeolite destruction	[8]
CO oxidation, gas turbine exhaust	N_2, O_2, 400 ppm CO, 100–400 ppm SO_2	Pt/Al_2O_3	$2SO_3 + \gamma\text{-}Al_2O_3 \rightarrow Al_2(SO_4)_3$ which blocks catalyst pores	[8]
Fischer–Tropsch	CO, H_2, H_2O, CO_2, HCs	Fe/K/Cu/SiO_2	$Fe_5C_2 \rightarrow Fe_3O_4$ due to oxidation at high X_{CO} by products H_2O, CO_2	[99]
Fischer–Tropsch	CO, H_2, H_2O, HCs	Co/SiO_2	$Co + SiO_2 \rightarrow CoO{\cdot}SiO_2$ and collapse of SiO_2 by product H_2O	[100]
Steam reforming and regeneration in H_2O	CH_4, H_2O, CO H_2, CO_2	Ni/Al_2O_3	$Ni + Al_2O_3 \rightarrow Ni_2Al_2O_4$	[8]

these metal catalysts is oxidized, sulfided or carbided, it will lose essentially all of its activity. While these chemical modifications are closely related to poisoning, the distinction here is that rather than losing activity due to the presence of an adsorbed species, the loss of activity is due to the formation of a new phase altogether.

Examples of vapor-induced chemical transformations of catalysts to inactive phases are listed in Table 10 [8,97–100]. These include the formation of $RhAl_2O_4$ in the three-way Pt-Rh/Al_2O_3 catalyst during high temperature operation in an auto exhaust; oxidation of Fe by low levels of O_2 during ammonia synthesis or by H_2O during regeneration; dealumination (migration of Al from the zeolite framework) of Y-zeolite during high temperature catalytic cracking and regeneration in steam; formation of aluminum sulfate and subsequent plugging of pores of Pt/Al_2O_3 in the presence of SO_3 during CO oxidation in a gas turbine exhaust; oxidation of Fe_5C_2 to Fe_3O_4 and of Co metal supported on silica to Co surface silicates during FT synthesis at high conversions and hence high P_{H_2O}; and formation of $Ni_2Al_2O_4$ during reaction and steam regeneration of Ni/Al_2O_3 in a slightly oxidizing atmosphere above about 500°C, especially if more reactive alumina, e.g. γ, δ, or θ forms, are used as supports. The reaction of SO_3 with γ-Al_2O_3 to produce $Al_2(SO_4)_3$ is also a serious cause of deactivation of alumina-supported catalysts for selective catalytic reduction (SCR) of nitrogen oxides (NO_x); hence, TiO_2 or SiO_2 is used as the carrier for V_2O_5 NO_x removal catalysts.

2.4.1.2. Reactions of gas/vapor with solid to produce volatile compounds. Metal loss through direct vaporization is generally an insignificant route to catalyst deactivation. By contrast, metal loss through formation of volatile compounds, e.g. metal carbonyls, oxides, sulfides and halides in CO, O_2, H_2S, and halogen-containing environments, can be significant over a wide range of condition, including relatively mild conditions. Classes and examples of volatile compounds are listed in Table 11. Carbonyls are formed at relatively low temperature but high pressures of CO; halides can be formed at relatively low temperatures and low concentration of the halogens. However, the conditions under which volatile oxides are formed vary considerably with the metal; for example, RuO_3 can be formed at room temperature, while PtO_2 is formed at measurable rates only at temperatures exceeding about 500°C.

While the chemical properties of volatile metal carbonyls, oxides and halides are well known, there is surprisingly little information available on their rates of formation during catalytic reactions. There have been no reviews on this subject and relatively few reported studies to define the effects of metal loss on catalytic activity [26,101–114]; most of the previous work has focused on volatilization of Ru in automotive converters [101–104], nickel carbonyl formation in nickel catalysts during methanation of CO [106–112] or during CO chemisorption at 25°C [26,108], formation of Ru carbonyls during Fischer–Tropsch synthesis [109,110], and volatilization of Pt during ammonia oxidation on Pt-Rh gauze catalysts [113,114].

Results of selected studies are summarized in Table 12. Bartholomew [104] found evidence of significant (50%) Ru loss after testing of a Pd-Ru catalyst in an actual reducing automobile exhaust for 100 h, which he attributed to formation of a volatile ruthenium oxide and which was considered responsible at least in part for a significant loss (20%) of NO reduction activity.

Shen et al. [106] found that Ni/Al_2O_3 methanation catalysts deactivate rapidly during methanation at high partial pressures of CO (>20 kPa) and temperatures

Table 11
Types and examples of volatile compounds formed in catalytic reactions

Gaseous environment	Compound type	Example of compound
CO, NO	Carbonyls and nitrosyl carbonyls	$Ni(CO)_4$, $Fe(CO)_5$ (0–300°C)[a]
O_2	Oxides	RuO_3 (25°C), PbO (>850°C), PtO_2 (>700°C)
H_2S	Sulfides	MoS_2 (>550°C)
Halogens	Halides	$PdBr_2$, $PtCl_4$, PtF_6

[a] Temperatures of formation are listed in parenthesis.

Table 12
Documented examples of reactions of vapor with solid to produce volatile compounds

Catalytic process	Catalytic solid	Vapor formed	Comments on deactivation process	References
Automotive converter	Pd-Ru/Al_2O_3	RuO_4	50% loss of Ru during 100 h test in reducing automotive exhaust	[104]
Methanation of CO	Ni/Al_2O_3	$Ni(CO)_4$	$Ni(CO)_4$ formation at $P_{CO} > 20$ kPa and $T < 425$°C diffusion and decomposition on the support as large crystallites	[106]
CO chemisorption	Ni catalysts	$Ni(CO)_4$	$Ni(CO)_4$ formation at $P_{CO} > 0.4$ kPa and $T > 0$°C catalyzed by sulfur compounds	[107]
Fischer–Tropsch synthesis	Ru/NaY-zeolite, Ru/Al_2O_3, Ru/TiO_2	$Ru(CO)_5$, $Ru_3(CO)_{12}$	Loss of Ru during FTS ($H_2/CO = 1$, 200–250°C, 1 atm) on Ru/NaY-zeolite and Ru/Al_2O_3; up to 40% loss while flowing CO at 175–275°C over Ru/Al_2O_3 for 24 h; rate of Ru loss less on titania-supported Ru and for catalysts containing 3 nm relative to 1.3 nm; surface carbon lowers loss	[109,110]
Ammonia oxidation	Pt-Rh gauze	PtO_2	Loss: 0.05–0.3 g Pt/t HNO_3; recovered with Pd gauze; loss of Pt leads to surface enrichment with inactive Rh	[8,116]
HCN synthesis	Pt-Rh gauze	PtO_2	Extensive restructuring and loss of mechanical strength	[8,120]

below 425°C due to $Ni(CO)_4$ formation, diffusion and decomposition on the support as large crystallites; under severe conditions (very high P_{CO} and relatively low reaction temperatures) loss of nickel metal occurs. Thus, loss of nickel and crystallite growth are serious problems at the entrance to methanation reactors where the temperature is low enough and P_{CO} high enough for metal carbonyl formation. Agnelli et al. [112] investigated kinetics and modeling of sintering due to formation and migration of nickel carbonyl species. They found that the initially sharp crystallite size distribution evolved during several hours of sintering under low temperature (230°C) reaction conditions to a bimodal system consisting of small spherical crystallites and large faceted crystals favoring (1 1 1) planes. The sintering process was modeled in terms of an Ostwald-ripening mechanism coupled with mass transport of mobile subcarbonyl intermediates. Long term simulations were found to predict reasonably well the ultimate state of the catalyst. Based on their work, they proposed two solutions for reducing loss of nickel: (1) increasing reaction temperature and decreasing CO partial pressure in order to lower the rate of carbonyl formation, and (2) changing catalyst composition, e.g. alloying nickel with copper or adding alkali to inhibit carbonyl species migration.

Loss of nickel metal during CO chemisorption on nickel catalysts at temperatures above 0°C is also a serious problem; moreover, this loss is catalyzed by sulfur poisoning [26]. In view of the toxicity of nickel tetracarbonyl, the rapid loss of nickel metal, and the ill-defined adsorption stoichiometries, researchers are advised to avoid using CO chemisorption for measuring nickel surface areas; instead, hydrogen chemisorption, an accepted ASTM method with a well-defined adsorption stoichiometry is recommended [115]. Fig. 19 illustrates a mechanism for the formation of $Ni(CO)_4$ on a crystallite of nickel in CO atmosphere.

Goodwin and co-workers [109,110] studied the influence of reaction atmosphere, support and metal particle size on the loss of Ru due to carbonyl formation. They found that the loss of Ru during CO hydrogenation ($H_2/CO = 1$; 200–250°C; 1 atm) on Ru/NaY-zeolite and Ru/Al_2O_3 for extended periods of time was significant (e.g. up to 40% while flowing CO at 175–275°C over Ru/Al_2O_3 for 24 h). The loss of Ru was significantly less on titania-supported Ru; moreover, the rate of loss was lower for catalysts

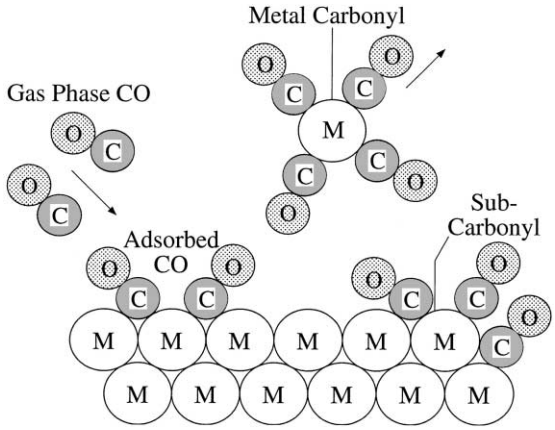

Fig. 19. Formation of volatile tetra-nickel carbonyl at the surface of nickel crystallite in CO atmosphere.

containing large metal crystallites (3 nm) relative to those containing small metal crystallites (1.3 nm). Moreover, metal loss was inhibited in part at higher reaction temperatures as a result of carbon deposition. Thus, while it is clear that loss of ruthenium could be a serious problem in Fischer–Tropsch synthesis, there are measures in terms of catalyst design and choice of reaction conditions that can be taken to minimize loss.

One of the most dramatic examples of vapor phase loss of the catalyst occurs during NH_3 oxidation on Pt-Rh gauze, an important reaction in the manufacture of nitric oxide [8,113,114]. At the high reaction temperature (~900°C), formation of a volatile platinum oxide (PtO_2) occurs at a very significant rate; in fact, the rate of loss of 0.05–0.3 g Pt/t of HNO_3 is high enough to provide a substantial economic incentive for Pt recovery [8]. The most effective recovery process involves placing a woven Pd-rich alloy gauze immediately below the Pt-Rh gauze to capture the Pt through formation of a Pd–Pt alloy. Pt loss is also the most significant cause of catalyst deactivation as the gauze surface becomes enriched in non-volatile but inactive rhodium oxide [116], requiring shutdown and catalyst replacement every 3–12 months [8].

Decomposition of volatile platinum oxide species formed during high temperature reaction may (similar to the previously discussed formation of large crystallites of Ni from $Ni(CO)_4$) lead to formation of large Pt crystallites and/or substantial restructuring of the metal surface. For example, Wu and Phillips

[117–119] observed surface etching, enhanced sintering, and dramatic surface restructuring of Pt thin films to faceted particles during ethylene oxidation over a relatively narrow temperature range (500–700°C). The substantially higher rate of sintering and restructuring in O_2/C_2H_4 relative to that in non-reactive atmospheres was attributed to the interaction of free radicals such as HO_2, formed homogeneously in the gas phase, with the metal surface to form metastable mobile intermediates. Etching of Pt-Rh gauze in a H_2/O_2 mixture under the same conditions as Pt surfaces (600°C, $N_2/O_2/H_2 = 90/7.5/2.5$) was reported by Hess and Phillips [120]. A significant weight loss was observed in a laminar flow reactor with little change in surface roughness, while in an impinging jet reactor, there was little weight loss, but substantial restructuring of the surface to particle-like structures, 1–10 μm in diameter; these particles were found to have the same Pt-Rh composition as the original gauze. The nodular structures of about 10 μm diameter formed in these experiments are strikingly similar to those observed on Pt-Rh gauze after use in production of HCN at 1100°C in 15% NH_3, 13% CH_4 and 72% air (see Fig. 20). Moreover, due to the high space velocities during HCN production, turbulent, rather than laminar flow would be expected as in the impinging

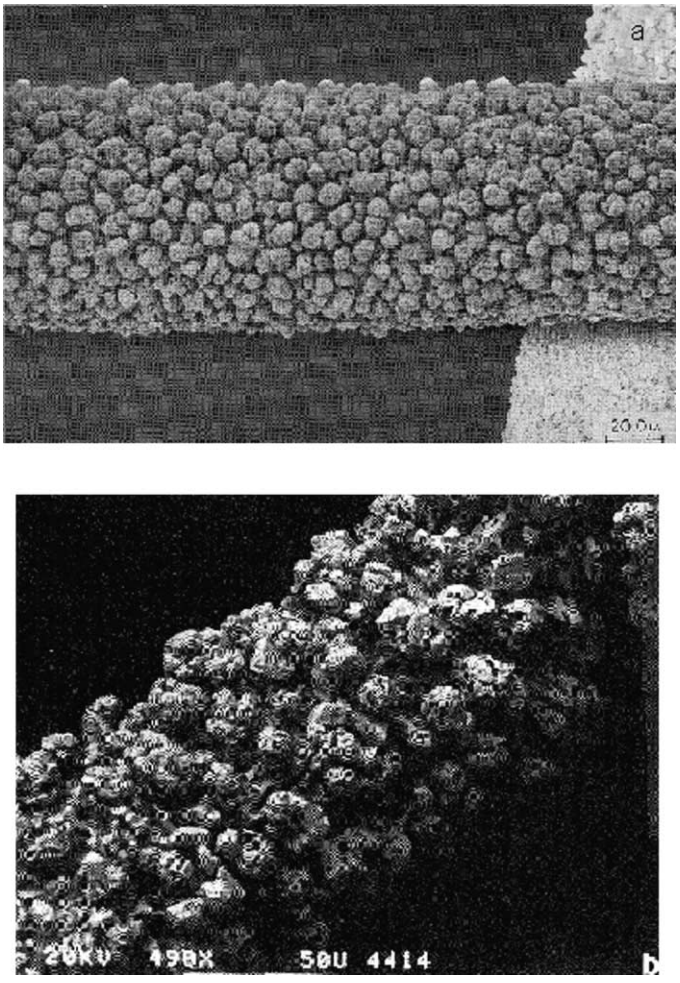

Fig. 20. (a) SEM of Pt-Rh gauze after etching in $N_2/O_2/H_2 = 90/7.5/2.5$ at 875 K for 45 h [120]. (b) SEM of Pt-Rh gauze after use in production of HCN; magnification: 1000× (photographs courtesy of Dr. Ted Koch at Du Pont).

jet reactor. While little Pt is volatilized from the Pt-Rh gauze catalyst during HCN synthesis, the extensive restructuring leads to mechanical weakening of the gauze [8].

Other examples of catalyst deactivation due to volatile compound formation include (1) loss of the phosphorus promoter from the VPO catalyst used in the fluidized-bed production of maleic anhydride with an attendant loss of catalyst selectivity [8], (2) vapor phase loss of the potassium promoter from steam-reforming catalysts in the high temperature, steam-containing environment [8], and (3) loss of Mo from a 12-Mo–V–heteropolyacid due to formation of a volatile Mo species during oxydehydrogenation of isobutyric acid to methacrylic acid [111].

While relatively few definitive studies of deactivation by volatile compound formation have been reported, the previous work does provide the basis for enumerating some general principles. A generalized mechanism of deactivation by formation of volatile metal compounds can be postulated (see Fig. 21). In addition, the roles of kinetics and thermodynamics can be stated in general terms:

1. At low temperatures and partial pressures of the volatilization agent (VA), the overall rate of the process is limited by the rate of volatile compound formation.
2. At intermediate temperatures and partial pressures of the VA, the rate of formation of the volatile compound exceeds the rate of decomposition. Thus, the rate of vaporization is high, the vapor is stable and metal loss is high.
3. At high temperatures and partial pressures of the VA, the rate of formation equals the rate of decomposition, i.e. equilibrium is achieved. However, the volatile compound may be too unstable to form or may decompose before there is an opportunity to be transported from the system. From the previous work, it is also evident that besides temperature and gas phase composition, catalyst properties (crystallite size and support) can play an important role in determining the rate of metal loss.

2.4.2. Solid-state reactions

Catalyst deactivation by solid-state diffusion and reaction appears to be an important mechanism for degradation of complex multi-component catalysts in dehydrogenation, synthesis, partial oxidation and total oxidation reactions [8,121–132]. However, it is difficult in most of these reactions to know the extent to which the solid-state processes such as diffusion and solid-state reaction are affected by surface reactions. For example, the rate of diffusion of Al_2O_3 to the surface to form an aluminate may be enhanced by the presence of gas phase oxygen or water or the nucleation of a different phase may be induced by either reducing or oxidizing conditions. Recognizing this inherent limitation, the focus here is nevertheless on processes in which formation of a new bulk phase

Generalized Mechanism:

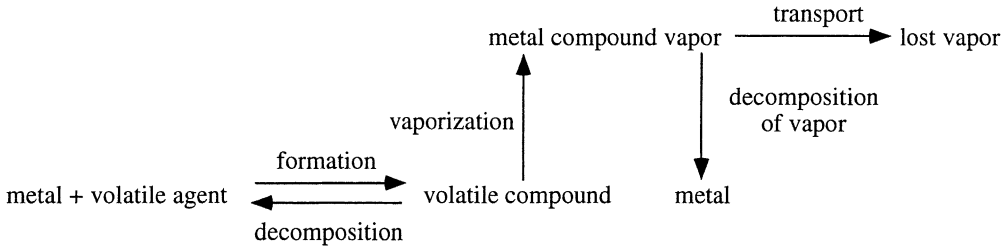

Generalized Kinetics:

a. rate of volatile compound formation = rate of formation - rate of decomposition

b. rate of metal loss = rate of vaporization - rate of vapor decomposition

Fig. 21. Generalized mechanisms and kinetics for deactivation by metal loss [8].

Table 13
Examples of solid-state transformations leading to catalyst deactivation

Catalytic process	Catalytic solid	Deactivating chemical reaction	References
Ammonia synthesis	$Fe/K/Al_2O_3$	Formation of $KAlO_2$ at catalyst surface	[131]
Catalytic combustion	PdO/Al_2O_3 PdO/ZrO_2	$PdO \rightarrow Pd$ at $T > 800^{\circ}C$	[124]
Catalytic combustion	Co/K on MgO, CeO_2, or La_2O_3	Formation of CoO-MgO solid solution, $LaCoO_3$, or K_2O film on CeO_2	[132]
Dehydrogenation of styrene to ethyl benzene	$Fe_2O_3/Cr_2O_3/K_2O$	K migration to center of pellet caused by thermal gradient	[8]
Fischer–Tropsch	Fe/K, Fe/K/CuO	Transformation of active carbides to inactive carbides	[129,130]
Oxidation of SO_2 to SO_3	$V_2O_5/K_2O/Na_2O$/kieselguhr	Formation of inactive V(IV) compounds at $T < 420$–$430^{\circ}C$	[127]
Partial oxidation of benzene to maleic anhydride	V_2O_5-MoO_3	Decreased selectivity due to loss of MoO_3 and formation of inactive vanadium compounds	[121]
Partial oxidation of methanol to formaldehyde	$Fe_2(MoO_4)_3$ plus MoO_3	Structural reorganization to β-$FeMoO_4$; reduction of MoO_3	[122,128]
Partial oxidation of propene to acrolein	$Fe_2(MoO_4)_3$	Reductive transformation of $Mo_{18}O_{52}$ to Mo_4O_{11}	[125,128]
Partial oxidation of isobutene to methacrolein	$Fe_2(MoO_4)_3$	Reduction to $FeMoO_4$ and MoO_{3-x}	[123,126]

(and presumably the attendant surface phase) leads to substantially lower activity. There is probably some overlap with some of the examples in Section 2.4.1.1 involving reactions of gas/vapor with solid to produce inactive phases.

Examples from the literature of solid-state transformations leading to catalyst deactivation are summarized in Table 13. They include (1) the formation during ammonia synthesis at the $Fe/K/Al_2O_3$ catalyst surface of $KAlO_2$, (2) decomposition of the active phase PdO to inactive Pd metal during catalytic combustion of PdO/Al_2O_3 and PdO/ZrO_2 catalysts, (3) transformation of active carbides to inactive carbides in Fischer–Tropsch synthesis on Fe/K/Cu catalysts, (4) formation of inactive V(IV) compounds in SO_2 oxidation, and (5) reductive transformation of iron molybdate catalysts during partial oxidation of benzene, methanol, propene, and isobutene.

There are basic principles underlying most solid-state reactions in working catalysts that have been enumerated by Delmon [128]: (1) the active catalytic phase is generally a high-surface area, defect structure of high surface energy and as such a precursor to more stable, but less active phases and (2) the basic reaction processes may themselves trigger the solid-state conversion of the active phase to an inactive phase; for example, it may involve a redox process, part of which nucleates the inactive phase.

A well-documented example of these principles occurs in the partial oxidation of propene to acrolein on a $Fe_2(MoO_4)_3$ catalyst [125,128]. This oxidation occurs by the "Mars van Krevelen" mechanism, i.e. a redox mechanism in which lattice oxygen reacts with the adsorbed hydrocarbon to produce the partially oxygenated product; the reduced catalyst is restored to its oxidized state through reaction with gaseous oxygen. In propene oxidation, two atoms of oxygen from the catalyst are used, one for removing two hydrogen atoms from the olefin and the other one in forming the unsaturated aldehyde. The fresh, calcined catalyst MoO_3 consists of corner-sharing MoO_6 octahedra (with Mo at the center and six oxygen atoms at the corners); but, upon reduction to MoO_2 octahedra share edges as shown in Fig. 22. However, it is reported [125,128] that only slightly reduced (relative to MoO_3), open structures such as $Mo_{18}O_{52}$ and Mo_8O_{23} are the most active, selective phases; more complete reduction of either of these structures leads to formation of Mo_4O_{11} (see Fig. 23) having substantially lower selectivity. Accordingly, over-reduction causes catalyst deactivation as structures of lower selectivity are formed. Delmon [126,128] have shown that addition of an oxygen donor such as Sb_2O_4 facilitates spillover of oxygen and thereby prevents over-reduction and deactivation of the catalyst.

2.5. Mechanical failure of catalysts

2.5.1. Forms and mechanisms of failure

Mechanical failure of catalysts is observed in several different forms, including (1) crushing of granular, pellet or monolithic catalyst forms due to a load, (2) attrition, the size reduction and/or breakup of catalyst granules or pellets to produce fines, especially in fluid or slurry beds, and (3) erosion of catalyst particles or monolith coatings at high fluid velocities. Attrition is evident by a reduction in the particle size or a rounding or smoothing of the catalyst particle

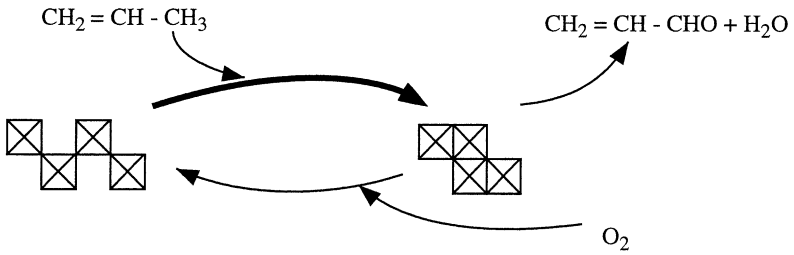

Fig. 22. Schematic representation of the cyclic reduction/oxidation of twin pairs of MoO_6 octahedra between the corner and the edge-sharing arrangements (boxes represent MoO_6 octahedra with sharing of oxygen atoms at corners for MoO_3 or edges for MoO_2). The figure is not completely accurate, because it cannot take into account the fact that the arrangements are not perpendicular to the main axes of the lattice [128].

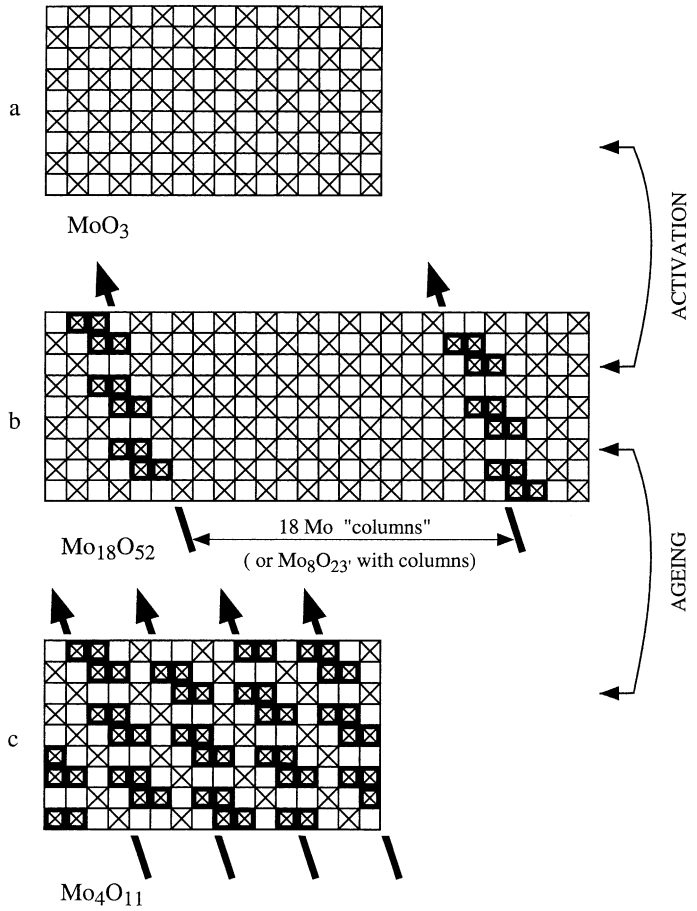

Fig. 23. Schematic representation of the structures of MoO_3, $Mo_{18}O_{52}$ and Mo_4O_{11}. The shear planes in $Mo_{18}O_{52}$ and Mo_4O_{11} are represented by the oblique arrows (boxes with an "X" represent MoO_5 octahedra) [128].

easily observed under an optical or electron microscope. Washcoat loss is observed by scanning the wall of the honeycomb channel with either an optical or electron microscope. Large increases in pressure drop in a catalytic process are often indicative of fouling, masking or the fracturing and accumulation of attrited catalyst in the reactor bed.

Commercial catalysts are vulnerable to mechanical failure in large part because of the manner in which they are formed; that is catalyst granules, spheres, extrudates, and pellets ranging in diameter from 50 μm to several centimeters are in general prepared by agglomeration of 0.02–2 μm aggregates of much smaller primary particles having diameters of 10–100 nm by means of precipitation or gel formation followed by spray drying, extrusion, or compaction. These agglomerates have in general considerably lower strengths than the primary particles and aggregates of particles from which they are formed.

Two principal mechanisms are involved in mechanical failure of catalyst agglomerates: (1) fracture of agglomerates into smaller agglomerates of approximately $0.2d_0$–$0.8d_0$ and (2) erosion (or abrasion) of aggregates of primary particles having diameters ranging from 0.1 to 10 mm from the surface of the agglomerate [133]. While erosion is caused by mechanical stresses, fracture may be due to mechanical, thermal and/or chemical stresses. Mechanical stresses leading to fracture or erosion in fluidized or slurry beds may result from (1) collisions of particles with

each other or with reactor walls or (2) shear forces created by turbulent eddies or collapsing bubbles (cavitation) at high fluid velocities. Thermal stresses occur as catalyst particles are heated and/or cooled rapidly; they are magnified by temperature gradients across particles and by differences in thermal expansion coefficients at the interface of two different materials, e.g. catalyst coating/monolith interfaces; in the latter case the heating or cooling process can lead to fracture and separation of the catalyst coating. Chemical stresses occur as phases of different density are formed within a catalyst particle via chemical reaction; for example, carbiding of primary iron oxide particles increases their specific volume and micro-morphology leading to stresses that break up these particles [134]. A further example occurs in supported metal catalysts when large quantities of filamentous carbon (according to reaction mechanisms discussed in Section 2.2) overfill catalysts pores generating enormous stresses which can fracture primary particles and agglomerates.

2.5.2. Role of physical and chemical properties of ceramic agglomerates in determining strength and attrition resistance

2.5.2.1. Factors affecting the magnitude of stress required for agglomerate breakage and the mechanisms by which it occurs. The extent to which a mechanism, i.e. fracture or erosion, participates in agglomerate size reduction depends upon several factors: (1) the magnitude of a stress, (2) the strength and fracture toughness of the agglomerate, (3) agglomerate size and surface area, and (4) crack size and radius. Erosion (abrasion) occurs when the stress (e.g. force per area due to collision or cavitation pressure) exceeds the agglomerate strength, i.e. the strength of bonding between primary particles. Erosion rate is reportedly [133] proportional to the external surface area of the catalyst; thus, erosion rate increases with decreasing agglomerate size.

2.5.2.2. Fracture toughness of ceramic agglomerates. Most heterogeneous catalysts are complex, multiphase materials which consist in large part of porous ceramic materials, i.e. are typically oxides, sulfides, or metals on an oxide carrier or support. When a tensile stress of a magnitude close to the yield point is applied, ceramics almost always undergo brittle fracture before plastic deformation can occur. Brittle fracture occurs through formation and propagation of cracks through the cross-section of a material in a direction perpendicular to the applied stress. Agglomerate fracture due to a tensile stress occurs by propagation of internal and surface flaws; these flaws created by external stresses or inherent defects are stress multipliers, i.e. the stress is multiplied by $2(a/r)^{0.5}$, where a is the crack length and r is the radius of curvature of the crack tip; since a/r can vary from 2 to 1000, the effective stress at the tip of a crack can be 4–60 times the applied stress. Tensile stress multipliers may be microcracks, internal pores, and grain corners.

The ability of a material to resist fracture is termed fracture toughness. The plain strain fracture toughness K_{Ic} is defined as

$$K_{Ic} = Y\sigma(\pi a)^{0.5} \tag{3}$$

where Y is a dimensionless parameter (often close to 1.0–2.0) the magnitude of which depends upon both specimen and crack geometries, σ the applied stress, and a is the length of a surface crack or half the length of an internal crack. Crack propagation and fracture are likely if the right-hand side of Eq. (3) exceeds the experimental value of plain strain fracture toughness (left-hand side of Eq. (3)). Plane strain fracture toughness values for ceramic materials are significantly smaller than for metals and typically below $10\,\text{MPa(m)}^{0.5}$; reported values for non-porous, crystalline alumina (99.9%), fused silica, and zirconia (3 mol% Y_2O_3) are 4–6, 0.8, and 7–12 $\text{MPa(m)}^{0.5}$, respectively; flexural strengths (analogous to yield strengths for metals) for the same materials are 280–550, 100, and 800–1500 MPa [135]. Thus, based on both fracture toughness and flexural strength, non-porous, crystalline zirconia is much stronger towards fracture than alumina which in turn is much stronger than fused silica.

2.5.2.3. Effects of porosity on ceramic agglomerate strength. The introduction of porosity to crystalline or polycrystalline ceramic materials will on the basis of stress amplification significantly decrease elastic modulus and flexural strength for materials in tension. This is illustrated by data in Fig. 24 showing that elastic modulus and flexural strength of a ceramic alumina (probably α form) are reduced 75 and 85%,

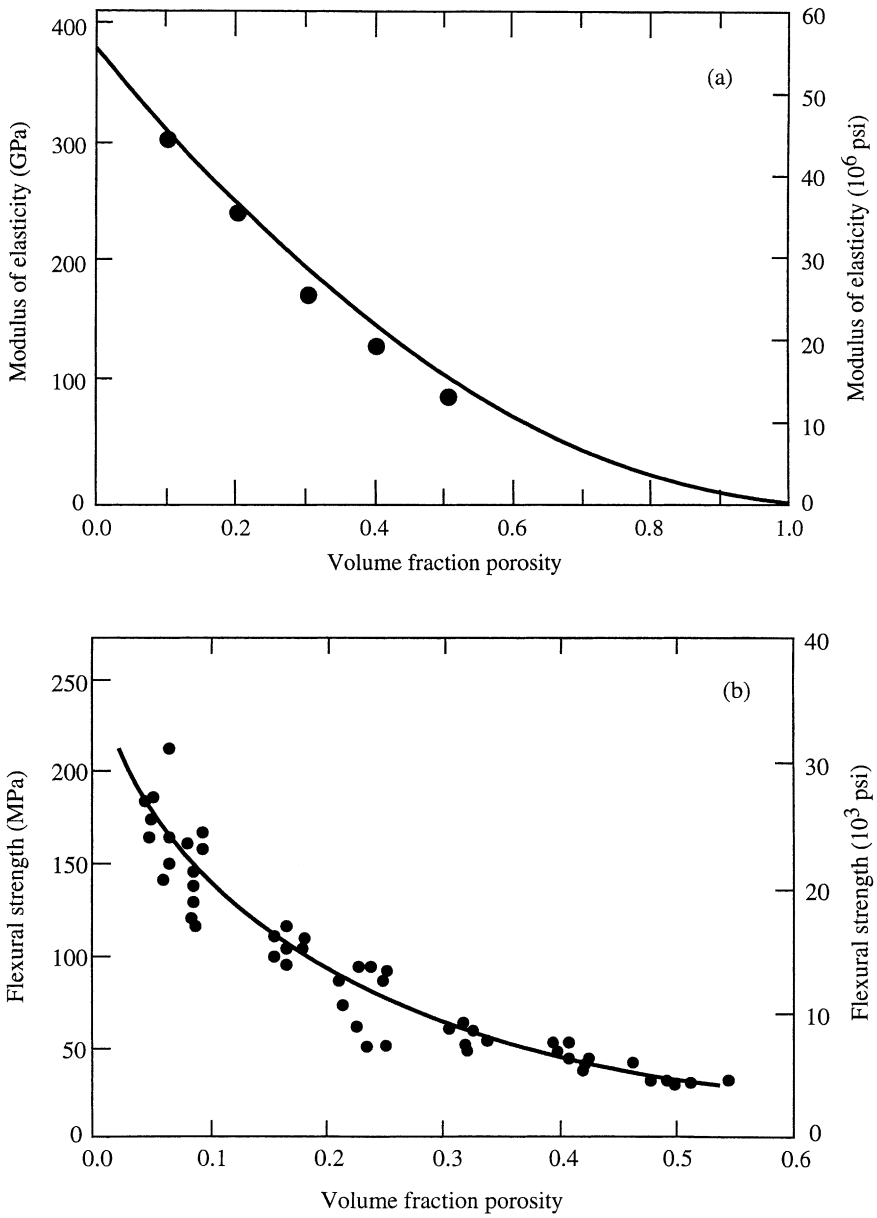

Fig. 24. The influence of porosity on (a) the modulus of elasticity for aluminum oxide at room temperature and (b) the flexural strength for aluminum oxide at room temperature [136].

respectively, as porosity is increased from 0 to 50% [136]. Thus, according to Fig. 24b the flexural strength of typical porous alumina used as catalyst supports might lie in the range of 30–40 MPa. However, yield strengths for γ-Al_2O_3, shown below in Section 2.5.3, are factors of 3–50 lower. Nevertheless, the data in Fig. 24b suggest that higher strengths may be possible.

2.5.2.4. Compressive strengths of ceramic materials. Thus far, the discussion has focused mainly on tensile strength, the extent of which is greatly reduced

by the presence of cracks or pores. However, for ceramic materials in compression, there is no stress amplification due to flaws or pores; thus ceramic materials (including catalytic materials) in compression are much stronger (approximately a factor of 10) than in tension. In addition, the strength of ceramic materials can be dramatically enhanced by imposing a residual compressive stress at the surface through thermal or chemical tempering. Moreover, introduction of binders such as graphite enables agglomerates of ceramic powders to undergo significant plastic deformation before fracture.

2.5.3. Tensile strengths and attrition resistance of catalyst supports and catalysts

2.5.3.1. Tensile strength data for catalyst support agglomerates. The strengths cited above for non-porous, annealed crystalline or polycrystalline materials do not necessarily apply to porous catalyst agglomerates even under compression; rather, agglomerate strength is dependent upon the strengths of chemical and physical bonds including the cohesive energy between primary particles. Agglomerate strength would depend greatly on the preparation of the compact. Representative data for catalyst agglomerates (see Table 14) suggest they are generally substantially weaker than polycrystalline ceramic materials prepared by high temperature sintering, such as alumina cited in Fig. 24 [133,135,137–141]. For example, Pham et al. [133] found that the breaking strength of a VISTA-B alumina agglomerate during uniaxial compaction is in the range of 5–10 MPa — substantially lower than the reported values for heat-treated polycrystalline alumina of 280–550 MPa [135]. A large part of this difference (about 85–95%) can be attributed to porosity; however, the remaining 5–15% must be due to differences in bonding between primary particles. In other words, the bonds between primary particles in catalyst agglomerates (and some ceramic agglomerates prepared by similar methods) are typically physical in nature (e.g. involve van der Waals forces) while those in sintered polycrystalline ceramic agglomerates are principally chemical due

Table 14
Mechanical strengths and attrition rates of catalyst supports compared to those of sintered ceramic agglomerates

Catalyst support or ceramic	Preparation/pretreatment/properties	Strength (MPa)	Attrition index (wt.%/h)	Reference
High surface area catalyst supports				
γ-Al_2O_3, 1.2–4.25 mm spheres	Sol–gel granulation/dried 10 h at 40°C, calcined 3 h at 450°C/389 m^2/g, $d_{pore} = 3.5$ nm	11.6 ± 1.9	0.033	[137]
γ-Al_2O_3, 4.25 mm spheres	Alcoa LD-350	0.7	0.177	[137]
γ-Al_2O_3, 100 μm	VISTA-B-965-500C	6.2 ± 1.3		[133]
TiO_2 (anatase), 30 μm	Thermal hydrolysis/dried 110°C, calcined 2 h 500°C/92 m^2/g, <10 nm primary crystallites	28[a]		[138]
TiO_2 (anatase), 90 μm	Base precipitation/dried 110°C, calcined 2 h 500°C/81 m^2/g, 10–14 nm primary crystallites	15[a]		[138]
TiO_2 (75% anatase, 25% rutile)	Degussa P25, fumed/4 mm extrudates/48 m^2/g, $V_{pore} = 0.34$ cm^3/g, $d_{pore} = 21$ nm	0.9		[139]
TiO_2 (anatase)	Rhone-Poulenc DT51, precipitate/4 mm extrudates/92 m^2/g, $V_{pore} = 0.40$ cm^3/g, $d_{pore} = 8.65$ nm	0.9		[139]
Low surface area ceramics				
Al_2O_3	Spray dried with organic binder; plastic deformation observed	2.3		[140]
Al_2O_3	Heat treated (sintered), 99.9%	282–551		[135]
TiO_2 (rutile)	Partially sintered	194		[140]
ZrO_2 (yttria additive)	Commercial samples from three companies, spray-dried	0.035–0.43		[141]
ZrO_2 (3% Y_2O_3)	Heat treated (sintered)	800–1500		[135]

[a] Rough estimates from break points on relative density vs. log(applied pressure) curves; data are consistent with mass distribution vs. pressure curves from ultrasonic tests.

to solid bridging of primary particles. Thus, there appears to be considerable potential for strengthening catalyst agglomerates, since their strengths are typically factors of 3–50 lower than for conventional, heat-treated ceramics of similar porosity.

2.5.3.2. Effects of preparation and pretreatment on catalyst agglomerate strength. From the data in Table 14 it is further evident that even subtle differences in preparation and pretreatment also affect agglomerate strength. For example, spheres of γ-Al_2O_3 prepared by sol–gel granulation are substantially (17 times) stronger than commercial γ-Al_2O_3 spheres [136]. Moreover, 30 and 90 μm diameter particles of TiO_2 prepared by thermal hydrolysis or basic precipitation are 30 and 15 times stronger than commercially available 4 mm extrudates [138,139].

2.5.3.3. Attrition of catalyst agglomerates: mechanisms, studies and test methods. Catalyst attrition is a difficult problem in the operation of moving-bed, slurry-bed, or fluidized-bed reactors. Generally, stronger materials have greater attrition resistance; this conclusion is supported by representative data in Table 14 for γ-Al_2O_3 showing that the strength of the alumina prepared by sol–gel granulation is 17 times higher, while its attrition rate is 5 times lower. The mechanism by which attrition occurs (erosion or fracture) can vary with catalyst or support preparation, crush strength and with reactor environment; it can also vary with the mechanical test method. There is some evidence in the attrition literature supporting the hypothesis that in the presence of a large stress, weaker oxide materials are prone to failure by fracture, while stronger materials tend to erode. For example, in the fluid catalytic cracking process, as new silica-alumina/zeolite catalyst in the form of 50–150 μm spherical agglomerates is added to replace catalyst lost by attrition, the weaker agglomerates break up fairly rapidly by fracture into smaller subagglomerates, following which the stronger agglomerates are slowly abraded to produce fine particles of 1–10 μm [142]. However, there is also contrary evidence from Thoma et al. [138] showing that fracture may be the preferred mechanism for strong TiO_2 agglomerates, while abrasion is favored for weaker agglomerates. That is, when subjected to ultrasonic stress, 30 μm diameter agglomerates of amorphous anatase (TiO_2) prepared by thermal hydrolysis were observed to undergo fracture to 5–15 μm fragments, while 90 μm agglomerates of polycrystalline anatase prepared by basic precipitation were found to break

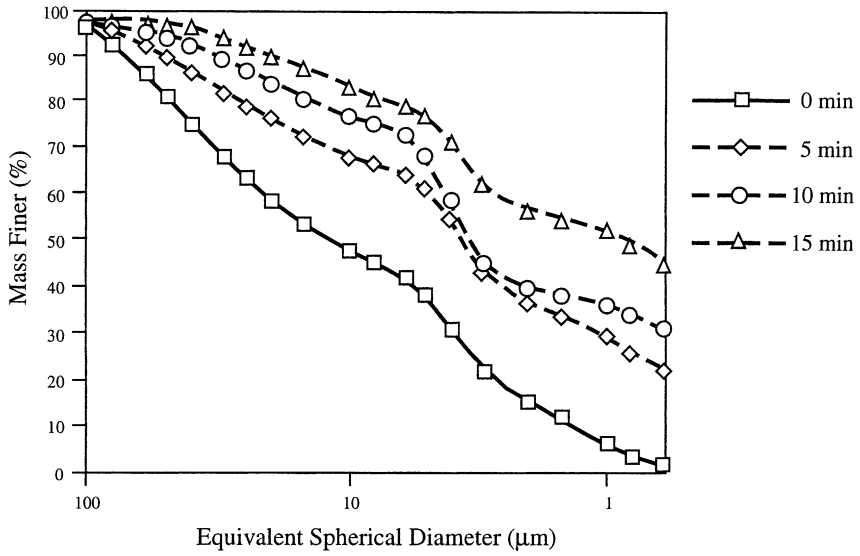

Fig. 25. Sedigraph particle size distribution for UCI FT catalyst UCI-LAPI-COMP-DRUMC, used previously in DOE pilot plant tests. There is considerable particle breakdown and generation of fine particles after 15 min of ultrasonic irradiation [133].

down by erosion to 0.1–5 μm fragments [138]; in this case the amorphous anatase was apparently stronger by a factor of 2 (see Table 14). Supporting a third trend, data from Pham et al. [133] show that attrition mechanism and rate are independent of agglomerate strength but depend instead on the type of material. That is, 100 μm diameter agglomerates of precipitated Fe/Cu/K Fischer–Tropsch catalyst (prepared by United Catalyst (UCI)) and having nearly the same strength shown in Table 14 for VISTA-B Al_2O_3 (6.3 versus 6.2 MPa), were found to undergo substantial fracture to 5–30 μm fragments (an increase from 45 to 85%, see Fig. 25) as well as substantial erosion to 1 μm or less fragments (increase from 2 to 50%). Under the same treatment conditions, 90 μm diameter agglomerates of VISTA-B Al_2O_3 underwent by comparison much less attrition, mainly by erosion (20% increase in 0.1–5 μm fragments). The very low attrition resistance of the Fe/Cu/K UCI catalyst is further emphasized by the unhappy outcome of a test by the US Department of Energy (DOE) of this catalyst in a pilot-scale slurry phase bubble-column reactor in LaPorte, TX; following 1 day of operation, the filter system was plugged with catalyst fines, preventing catalyst-wax separation and forcing shutdown of the plant [143].

Thus, based on these three representative examples, it follows that which of the two attrition mechanisms predominates depends much more on material composition and type than on agglomerate strength. However, irrespective of mechanism the rate of attrition is usually greater for the weaker material.

Fig. 26 illustrates the large effect that catalyst preparation method can have on the attrition resistance of an Fe/Cu Fischer–Tropsch catalyst [144]. This catalyst, prepared by precipitation, undergoes severe attrition during a 25 min treatment with ultrasonic radiation; indeed the mass fraction finer than 0.1–5 μm increases from 0 to 65%. However, after a spray drying treatment of the same catalyst, less than a 10% increase in the same fractions is evident.

In their review of attrition and attrition test methods, Bemrose and Bridgwater [145] discuss how attrition varies with reactor type, e.g. involves mainly particle–wall impacts in moving pellet bed reactors and particle–particle impacts in fluidized-bed reactor of high fluid velocity. In fact, jet attrition of catalyst particles in a gas fluidized bed involving principally abrasion due to collision of high-velocity particles has

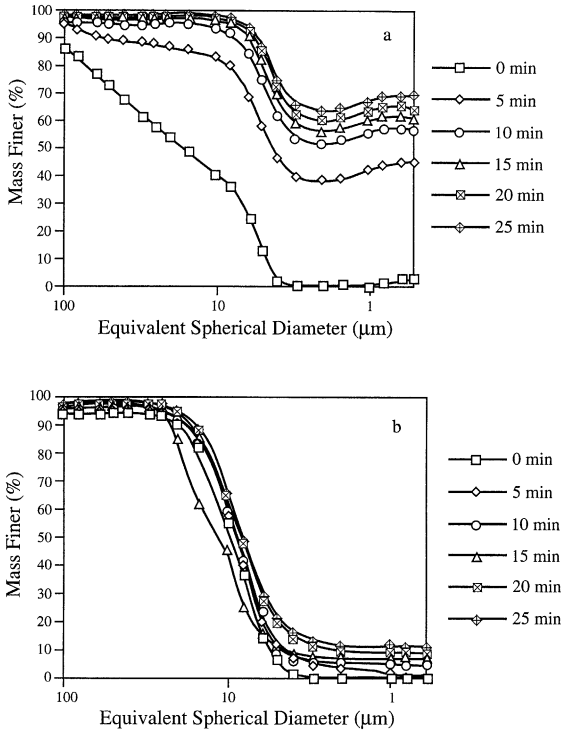

Fig. 26. Sedigraph particle size distributions of a precipitated Fe-Cu catalyst, as-prepared and after spray-drying. The as-prepared catalyst (a) is weak and breaks down easily after 25 min of ultrasonic irradiation, while spray-drying (b) improves its attrition resistance [144].

been modeled in some detail [142,146]. Thus, given such important differences in attrition mechanism, realistic attrition test methods should attempt to model reactor operation as closely as possible. In addition, the ideal test would require only a small catalyst sample, a simple, inexpensive apparatus, and a few minutes to complete the test. Relatively quick, inexpensive single particle crushing tests have been devised [145], however, properties of a single particle are rarely representative of those for the bed; moreover, it is difficult to relate the results of this crushing test to the actual abrasion process. Realistic tests have been devised for two reactor types involving a moving catalyst, i.e. an air-jet test for fluidized-bed catalysts [147,148], and a rotating drum apparatus for moving-bed catalysts [149]; however, the air-jet test requires a large quantity (e.g. 50 g) of catalyst, an expensive apparatus, and about 20 h to run. In the past decade a new jet-cup test

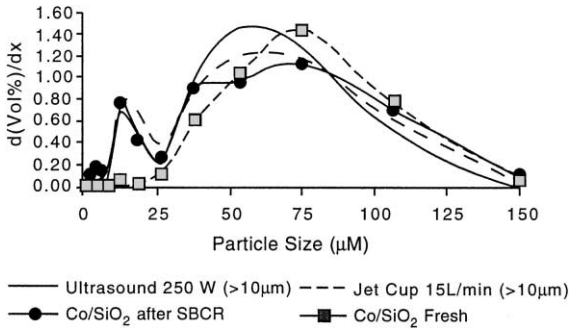

Fig. 27. Particle size distributions of Co/SiO_2 catalyst [148].

has been developed for testing of fluidized-bed catalysts [147,148] which requires only a 5 g sample and about 1 h to complete; comparisons of results for the jet-cup and air-jet tests indicate that the two tests give comparable results [147,148]. Nevertheless, the mechanisms for the two tests are different, i.e. the air-jet (fluid-bed) test is abrasion (erosion)-dominant, while the jet-cup test includes both abrasion and fracture mechanisms [148]. A 30 min, 10 g ultrasonic attrition test based on cavitation has also been developed in the past decade [133,138,150]; while it likewise involves both abrasion and fracture mechanisms, the results appear to correlate with other methods. For example, particle size distributions for the same Co/silica catalyst after ultrasonic, jet-cup and lab-scale, slurry-bed column reactor (SBCR) tests are very similar (see Fig. 27) indicating that both fracture and abrasion mechanisms operate in the small-scale SBCR. Moreover, the good agreement among the three methods suggests that both the jet-cup and ultrasonic tests may provide data representative of the attrition process in lab-scale SBCR reactors. It is evident that these two small-scale methods are especially useful for screening of a series of catalysts to determine relative strength.

Nevertheless, the more realistic large-scale tests are probably needed for accurately determining design attrition rates of a commercial catalyst to be used in a full-scale process. The observation that attrition of an FCC catalyst initially involves fracture of weak agglomerates followed by abrasion of strong agglomerates emphasizes the need to collect and analyze the particle size distribution of attrited fines as a function of time in order to define which mechanism (or mechanisms) operates at startup as well as in the steady-state process. Because the mechanism may be time dependent, rapid, small-scale tests may produce misleading results.

While realistic lab-scale tests have been developed for simulating attrition in large moving-bed and fluidized-bed reactors, no such laboratory test has been developed and demonstrated yet for simulation of large-scale SBCR reactors, although recent research has focused on the development of such tests. For example, in lab-scale, SBCR tests of supported cobalt catalysts over several days [150], it was observed that the attrition resistance decreases in the order Co/Al_2O_3, Co/SiO_2, Co/TiO_2 (especially the anatase form underwent attrition at a high rate); attrition resistance was observed to increase with increasing cobalt loading from 10 to 40 wt.%.

2.5.4. Implications of mechanistic knowledge of attrition for catalyst design

The understanding of mechanisms important in attrition of catalyst supports and catalysts, the relationship between strength and attrition rate for a given material, and test data can be used to great advantage in the design of attrition resistant catalysts. Several alternatives follow from the previous discussion for increasing attrition resistance: (1) increasing aggregate/agglomerate strength by means of advanced preparation methods, e.g. sol–gel granulation, spray drying, and carefully controlled precipitation methods (see Table 14 and Fig. 26 for examples), (2) adding binders to improve strength and toughness, e.g. the addition of a polyvinylpyrrolidone binder to agglomerates of quartz sand increases agglomerate strength from 0.1 to 3 MPa [151], (3) coating aggregates with a porous but very strong material such as ZrO_2, e.g. embedding a fluidized-bed catalyst for partial oxidation of *n*-butane to maleic anhydride in a strong, amorphous matrix of zirconium hydrogen phosphate significantly improves its attrition resistance [152], and (4) chemical or thermal tempering of agglomerates to introduce compressive stresses which increase strength and attrition resistance, e.g. heating and cooling particles rapidly by passing them through a low-residence-time, high-temperature furnace to harden the agglomerate exterior, while preventing significant sintering of or phase changes in the porous interior.

3. Summary, perspective, and needs for further investigation

3.1. Summary

This review summarizes the present state of knowledge regarding catalyst deactivation mechanisms. Important facts and conclusions can be summarized as follows:

1. The mechanisms of catalyst deactivation are many; nevertheless, they can be grouped into six intrinsic mechanisms of catalyst decay: (i) poisoning, (ii) fouling, (iii) thermal degradation, (iv) vapor compound formation accompanied by transport, (v) vapor–solid and/or solid–solid reactions, and (vi) attrition/crushing. As (i), (iv), and (v) are chemical in nature while (ii) and (v) are mechanical, the causes of deactivation are basically three-fold: chemical, mechanical and thermal.
2. Poisoning is the strong chemisorption of reactants, products or impurities on sites otherwise available for catalysis. Depending upon the poison concentration, poisoning may be rapid or slow; depending on the strength of poison adsorption, poisoning may be reversible or irreversible. Mechanistically, poisoning is a complex process involving some or all of the following: (a) physical blockage of one or more catalytic sites by the strongly adsorbed poison, (b) electronic modification of nearest neighbor atoms and sometimes even next-nearest neighbor atoms, (c) restructuring of the adsorbent surface, and (d) hindering surface diffusion of adsorbed reactants, thereby preventing reaction. Since a number of common poisons such as coke, sulfur and arsenic compounds are strongly and irreversibly adsorbed, poisoning is best prevented through purification of the reactant stream by means of scrubbers or guard beds, rather than attempting to remove the poison from the catalyst after the fact.
3. Fouling is the physical (mechanical) deposition of species from the fluid phase onto the catalyst surface, which results in activity loss due to blockage of sites and/or pores. In its advanced stages it may result in disintegration of catalyst particles and plugging of the reactor voids. Important examples include (a) copious deposits of filamentous carbon due to CO disproportionation during operation at relatively high temperatures and/or at low H_2/CO or steam/C ratios in Fischer–Tropsch synthesis, methanation, and steam reforming of methane and (b) multilayer accumulation of coke in catalytic cracking on zeolites or hydrotreating on $CoMo/Al_2O_3$ catalysts. Carbon deposition and coke formation occur at relatively low rates under favorable reaction conditions; however, under unfavorable conditions, high rates can lead to catastrophic failure of the catalyst and plugging of reactor voids leading to shutdown within hours. Mechanistically, carbon deposition on supported metals and coke formation on zeolites are very different. The former involves dissociation of CO or hydrocarbons on the metal surface to form α-carbon which can then polymerize to undesirable carbon forms such as graphite or carbon filaments. The latter (coke formation on zeolites) occurs by a series of free radical carbocation reactions on acid sites including dehydrogenation, oligomerization, cyclization, aromatization, and formation of polynuclear aromatics. Keys to preventing carbon deposition and coke formation include: (a) operating under conditions that minimize formation, e.g. at sufficiently high H_2/CO ratios in FT synthesis so that precursors to inactive carbon formation are kept at a low coverage by gasification with hydrogen; (b) optimizing catalyst design, e.g. in the case of zeolites optimizing acidity to minimize coke formation; and (c) purifying the feed to remove precursors that accelerate carbon or coke formation, e.g. removal of polynuclear aromatics from the feed of a hydrocracking or hydrotreating process which otherwise react readily on acid sites to form coke. Where coke formation is not easily prevented (e.g. catalytic cracking and reforming) deactivation is relatively easily reversed by regeneration through carefully controlled low-temperature combustion of deposited coke in air.
4. Thermally-induced deactivation of catalysts result from (i) loss of catalytic surface area due to crystallite growth of the catalytic phase, (ii) loss of support area due to support collapse and of catalytic surface area due to pore collapse on crystallites of the active phase, and/or (iii) chemical transformations of catalytic phases to non-catalytic phases. The first two processes are typically referred to as “sintering”. Sintering processes generally take place at high reaction temperatures (e.g. >500°C)

and are generally accelerated by the presence of water vapor. Three principal mechanisms of metal crystallite growth have been advanced: (1) crystallite migration, (2) atomic migration, and (3) (at very high temperatures) vapor transport. Redispersion, the reverse of crystallite growth in the presence of O_2 and/or Cl_2, may involve (a) formation of volatile metal oxide or metal chloride complexes which attach to the support and are subsequently decomposed to small crystallites upon reduction and/or (b) formation of oxide particles or films that break into small crystallites during subsequent reduction. Growth of metal crystallites on a support could in principle involve a combination of all three sintering mechanisms operating simultaneously, although relative rates will depend upon reaction conditions. Temperature, atmosphere, metal type, metal dispersion, promoters/impurities and support surface area, texture and porosity, are the principal parameters affecting rates of sintering and redispersion. Sintering rates increase exponentially with temperature; activation energies are on the order of 15–100 kJ/mol. Metals sinter relatively rapidly in oxygen or water vapor and relatively slowly in hydrogen. Promoters such as MgO or BaO lower sintering rates by decreasing metal atom mobility, while support surface defects or pores impeded surface migration of metal particles. In general, sintering processes are slow at moderate reaction temperatures and either irreversible or difficult to reverse. Thus, sintering is more easily prevented than cured; the key is to maximize catalytic activity enough to enable operation at temperatures low enough that sintering rates are negligible.

5. In addition to poisoning, there are other chemical routes leading to catalyst deactivation: (1) reactions of the vapor phase with the catalyst surface to produce (a) inactive bulk and surface phases (rather than strongly adsorbed species) or (b) volatile compounds which exit the catalyst and reactor in the vapor phase, (2) catalytic solid–support or catalytic solid–promoter reactions, and (3) solid-state transformations of the catalytic phases during reaction. Examples of these four phenomena include: (1) oxidation of Co metal supported on silica by product water to Co surface silicates during FT synthesis at high conversion, (2) loss of Pt by formation of volatile PtO_2 during ammonia oxidation on Pt-Rh gauze catalysts, (3) formation during ammonia synthesis at the $Fe/K/Al_2O_3$ catalyst surface of $KAlO_2$, and (4) reductive transformation of $Mo_{18}O_{52}$ to Mo_4O_{11} during partial oxidation of propene to acrolein. These forms of chemical deactivation can be prevented or moderated in large part through careful control of reaction conditions and appropriate design of the catalyst.
6. Mechanical failure of catalysts is observed in several different forms, including (1) crushing of granular, pellet or monolithic catalyst forms due to a load, (2) attrition, the size reduction and/or breakup of catalyst granules or pellets to produce fines, especially in fluid or slurry beds, and (3) erosion of catalyst particles or monolith coatings at high fluid velocities. Two principal mechanisms are involved in attrition of catalyst agglomerates: (1) fracture of agglomerates into smaller agglomerates of approximately $0.2d_0$–$0.8d_0$ and (2) erosion (or abrasion) of aggregates of primary particles having diameters ranging from 0.1 to 10 μm from the surface of the agglomerate. While erosion is caused by mechanical stresses, fracture may be due to mechanical, thermal and/or chemical stresses. Mechanical stresses leading to fracture or erosion in fluidized or slurry beds may result from (1) collisions of particles with each other or with reactor walls or (2) shear forces created by turbulent eddies or collapsing bubbles (cavitation) at high fluid velocities. The extent to which a mechanism, i.e. fracture or erosion, participates in agglomerate size reduction depends upon several factors: (1) the magnitude of a stress, (2) the strength and fracture toughness of the agglomerate, (3) agglomerate size and surface area, and (4) crack or pore size and radius. There appears to be considerable potential for strengthening catalyst agglomerates, since their strengths are typically factors of 3–50 lower than for conventional, heat-treated ceramics of similar porosity. Subtle changes in preparation, pretreatment, and fabrication can greatly improve catalyst agglomerate strength. Some promising alternatives for increasing catalyst attrition resistance and strength include (1) increasing aggregate/agglomerate strength by means of advanced preparation methods, e.g. sol–gel granulation, spray drying, and carefully controlled precipitation methods, (2) adding binders to improve strength

and toughness, (3) coating aggregates with a porous but very strong material such as ZrO_2, and (4) chemical or thermal tempering of agglomerates to introduce compressive stresses which increase strength and attrition resistance.

3.2. Perspective and needs for further investigation

The development during the past two decades of more sophisticated surface spectroscopies and powerful computer technologies provides opportunities for obtaining substantially better understanding of deactivation mechanisms and building this understanding into comprehensive mathematical models that will enable more effective design and optimization of processes involving deactivating catalysts. Presently, there are relatively few such comprehensive models that can be used by design engineers and plant operators. The status of knowledge and needs for further work are summarized below for each type of deactivation mechanism.

3.2.1. Poisoning

Poisoning of catalysts is a relatively well-studied, reasonably well-understood phenomenon. Poisoning by reversible and irreversible poisons can usually be modeled with moderate success at the process level. Nevertheless, the ability to quantitatively model at the molecular level (a) poison-surface atom binding energies and effects of poison adsorption on the binding energies of adjacent adsorbed reactants or (b) restructuring of surfaces due to adsorbed poisons is lacking. While structures of adsorbed poisons such as sulfur on metals in a vacuum have been well-characterized by surface science techniques, there are few such data (if any) for adsorbed poisons under reaction conditions. There is a paucity of data on the intrinsic effects of poisons on activities of well-defined catalyst systems measured during reaction in the absence of gas phase or solid phase concentration gradients.

3.2.2. Carbon and coke formation

The mechanisms by which various carbon species are formed on supported metals and by which various types of coke are formed on acidic oxides and sulfides are only moderately well understood. The structures of a number of carbon species (e.g. β-carbon formed during CO hydrogenation on metals) and coke deposits (e.g. types I–III) formed in hydrodesulfurization need to be better defined. Of even greater importance is research establishing specific links between the quantity of certain carbon or coke structures on the surface or in multilayers and the extent of deactivation. In addition, rate data are needed for the elementary steps involved in the formation of various carbons (α–γ) and coke molecules. Theoretical and empirical models are also needed for diffusion of small to large molecules in zeolite pores which include the effects of acidity and allow calculations of diffusivity. Once established these links and kinetic parameters will provide a fundamental basis for development of more effective models of catalyst deactivation by carbons and cokes. There is a need for better understanding of how noble metal promoters influence carbon and coke formation rates in CO hydrogenation and steam reforming. Likewise, the roles of acid strength and acid site density in coke formation on acidic oxides need to be better understood for a number of reactions.

3.2.3. Sintering

Development of comprehensive sintering models has suffered due to (a) the complexity of the elementary processes, (b) a lack of kinetic data for these processes, and (c) a lack of high quality dispersion and particle-size distribution versus time data needed for validating such models. Comprehensive, statistically-significant measurements of sintering rates for supported metal catalysts under reaction conditions over several hundreds of hours and where possible in large scale processes are needed for process design/optimization and model development/validation. While sophisticated spectroscopic tools have been used effectively during the past two decades to advance our fundamental understanding of sintering and redispersion, additional insights into atomic and molecular processes occurring during sintering and redispersion are needed to develop more sophisticated, realistic models.

3.2.4. Vapor–solid and solid-state reactions

There are relatively few catalytic reactions for which definitive studies of these deactivation processes have been carried out. There have been relatively few fundamental studies of these reactions for well-defined systems at the surface molecular level. There are a number of catalytic processes that might

benefit from such studies, e.g. partial oxidations on complex oxides and Fisher–Tropsch synthesis on cobalt and iron catalysts. For example, hydrothermal degradation of cobalt/alumina and cobalt/silica catalysts to form aluminates and silicates is a serious problem in FT synthesis at the high-pressure, high-conversion conditions typical of commercial operation. Some recent studies have addressed this problem, but there is a clear need for further definitive work to understand and treat this problem.

3.2.5. Mechanical failure

Mechanical failure due to attrition or collapse of agglomerates is a serious or limiting problem in many commercial catalytic processes. Yet our present understanding of these problems barely exceeds that taught in sophomore materials science. Effective test methods have been developed only in the last decade. The few available data suggest that significant improvements in the strengths and attrition resistances of catalyst agglomerates are possible through the use of more sophisticated preparation, pretreatment, and forming methods. There are critical needs for developing stronger, more attrition resistant catalytic materials, e.g. the need to develop attrition resistant FT catalysts for slurry bubble column operation.

References

[1] J.L. Figuerido (Ed.), Progress in Catalyst Deactivation, NATO Advanced Study Institute Series E, Marunus Nijhoff, Boston, 1982.
[2] R. Hughes, Deactivation of Catalysts, Academic Press, London, 1984 (Chapter 8).
[3] J. Oudar, H. Wise, Deactivation and Poisoning of Catalysts, Marcel Dekker, New York, 1985, p. 1.
[4] J.B. Butt, E.E. Petersen, Activation, Deactivation, and Poisoning of Catalysts, Academic Press, San Diego, 1988.
[5] P.J. Denny, M.V. Twigg, in: B. Delmon, G.F. Froment (Eds.), Catalyst Deactivation 1980, Stud. Surf. Sci. Catal., Vol. 6, Elsevier, Amsterdam, 1980, p. 577.
[6] C.H. Bartholomew, Chem. Eng. 91 (1984) 96.
[7] J.B. Butt, in: J.R. Anderson, M. Boudart (Eds.), Catalysis, Science and Technology, Springer, New York, 1984, p. 1.
[8] R.J. Farrauto, C.H. Bartholomew, Fundamentals of Industrial Catalytic Processes, Chapman & Hall, Kluwer Academic Publishers, London, 1997 (Chapter 5).
[9] B. Delmon, G.F. Froment, Catalyst Deactivation 1980, Stud. Surf. Sci. Catal., Vol. 6, Elsevier, Amsterdam, 1980.
[10] B. Delmon, G.F. Froment, Catalyst Deactivation 1987, Stud. Surf. Sci. Catal., Vol. 34, Elsevier, Amsterdam, 1987.
[11] C.H. Bartholomew, J.B. Butt, Catalyst Deactivation 1991, Stud. Surf. Sci. Catal., Vol. 68, Elsevier, Amsterdam, 1991.
[12] B. Delmon, G.F. Froment, Elsevier 1994, Stud. Surf. Sci. Catal., Vol. 88, Elsevier, Amsterdam, 1994.
[13] C.H. Bartholomew, G.A. Fuentes, Catalyst Deactivation 1997, Stud. Surf. Sci. Catal., Vol. 111, Elsevier, Amsterdam, 1997.
[14] B. Delmon, G.F. Froment, Catalyst Deactivation 1999, Stud. Surf. Sci. Catal., Vol. 126, Elsevier, Amsterdam, 1999.
[15] E.B. Maxted, Adv. Catal. 3 (1951) 129.
[16] L.L. Hegedus, R.W. McCabe, in: B. Delmon, G.F. Froment (Eds.), Catalyst Deactivation 1980, Stud. Surf. Sci. Catal., Vol. 6, Elsevier, Amsterdam, 1980.
[17] L.L. Hegedus, R.W. McCabe, Catalyst Poisoning, Marcel Dekker, New York, 1984.
[18] J.B. Butt, in: J.L. Figuerido (Ed.), Progress in Catalyst Deactivation, NATO Advanced Study Institute Series E, Marunus Nijhoff, Boston, 1982, p. 153.
[19] J. Barbier, in: J. Oudar, H. Wise (Eds.), Deactivation and Poisoning of Catalysts, Marcel Dekker, New York, 1985, p. 109.
[20] C.H. Bartholomew, in: B. Delmon, G.F. Froment (Eds.), Catalyst Deactivation 1987, Stud. Surf. Sci. Catal., Vol. 34, Elsevier, Amsterdam, 1987.
[21] J.R. Rostrup-Nielsen, in: C.H. Bartholomew, J.B. Butt (Eds.), Catalyst Deactivation 1991, Stud. Surf. Sci. Catal., Vol. 68, Elsevier, Amsterdam, 1991, p. 85.
[22] V.J. Volter, M. Hermann, Z. Anorg. Allg. Chem. 405 (1974) 315.
[23] K. Baron, Thin Solid Films 55 (1978) 449.
[24] R.D. Clay, E.E. Petersen, J. Catal. 16 (1970) 32.
[25] R.J. Madon, H. Shaw, Catal. Rev.-Sci. Eng. 15 (1977) 69.
[26] C.H. Bartholomew, P.K. Agrawal, J.R. Katzer, Adv. Catal. 31 (1982) 135.
[27] J.R. Rostrup-Nielsen, in: J.L. Figuerido (Ed.), Progress in Catalyst Deactivation, NATO Advanced Study Institute Series E, Marunus Nijhoff, Boston, 1982, p. 209.
[28] H. Wise, J. McCarty, J. Oudar, in: J. Oudar, H. Wise (Eds.), Deactivation and Poisoning of Catalysts, Marcel Dekker, New York, 1985, p. 1.
[29] J.R. Rostrup-Nielsen, P.E. Nielsen, in: J. Oudar, H. Wise (Eds.), Deactivation and Poisoning of Catalysts, Marcel Dekker, New York, 1985, p. 259.
[30] M. Perdereau, J. Oudar, Surf. Sci. 20 (1970) 80.
[31] J. Oudar, Catal. Rev.-Sci. Eng. 22 (1980) 171.
[32] J. Oudar, H. Wise, Deactivation and Poisoning of Catalysts, Marcel Dekker, New York, 1985, p. 1.
[33] J.J. McCarroll, T. Edmonds, R.C. Pitkethly, Nature 223 (1969) 1260.
[34] T. Edmonds, J.J. McCarroll, R.C. Pitkethly, J. Catal. Sci. Technol. 8 (1971) 68.
[35] J. Hepola, J. McCarty, G. Krishnan, V. Wong, Appl. Catal. B, 2001, in press.
[36] W. Erley, H. Wagner, J. Catal. 53 (1978) 287.
[37] K.D. Rendulic, A. Winkler, Surf. Sci. 74 (1978) 318.
[38] D.W. Goodman, M. Kiskinova, Surf. Sci. 105 (1981) L265.
[39] M. Kiskinova, D.W. Goodman, Surf. Sci. 108 (1981) 64.

[40] S. Johnson, R.S. Madix, Surf. Sci. 108 (1981) 77.
[41] R.J. Madix, M. Thornberg, S.B. Lee, Surf. Sci. 133 (1983) L447.
[42] E.L. Hardegree, P. Ho, J.M. White, Surf. Sci. 165 (1986) 488.
[43] E.J. Erekson, C.H. Bartholomew, Appl. Catal. 5 (1983) 323.
[44] J.R. Rostrup-Nielsen, D.L. Trimm, J. Catal. 48 (1977) 155.
[45] D.L. Trimm, Catal. Rev.-Sci. Eng. 16 (1977) 155.
[46] D.L. Trimm, Appl. Catal. 5 (1983) 263.
[47] C.H. Bartholomew, Catal. Rev.-Sci. Eng. 24 (1982) 67.
[48] L.F. Albright, R.T.K. Baker (Eds.), Coke Formation on Metal Surfaces, ACS Symposium Series 202, American Chemical Society, Washington, DC, 1982.
[49] P.G. Menon, J. Mol. Catal. 59 (1990) 207.
[50] J.D. Deken, P.G. Menon, G.F. Froment, G. Haemers, J. Catal. 70 (1981) 225.
[51] W.G. Durer, J.H. Craig Jr., J. Lozano, Appl. Surf. Sci. 45 (1990) 275.
[52] A.D. Moeller, C.H. Bartholomew, ACS Fuel Chem. Div. (Preprint) 25 (1980) 54.
[53] K.J. Marschall, L. Mleczko, Ind. Eng. Chem. Res. 38 (1999) 1813.
[54] J.R. Rostrup-Nielsen, in: J.R. Anderson, M. Boudart (Eds.), Catalysis Science and Technology, Springer, New York, 1984, p. 1.
[55] F. Besenbacher, I. Chorkendorff, B.S. Clausen, B. Hammer, A.M. Molenbroek, J.K. Norscov, I. Stensgaard, Science 279 (1998) 1913.
[56] T. Nemes, A. Chambers, R.T.K. Baker, J. Phys. Chem. 102 (1998) 6323.
[57] C.H. Bartholomew, M.V. Strasburg, H. Hsieh, Appl. Catal. 36 (1988) 147.
[58] C.K. Vance, C.H. Bartholomew, Appl. Catal. 7 (1983) 169.
[59] R.T.K. Baker, J.J. Chludzinski, J. Catal. 64 (1980) 464.
[60] D.E. Brown, J.T.K. Clark, A.I. Foster, J.J. McCarroll, M.L. Sims, in: L.F. Albright, R.T.K. Baker (Eds.), Coke Formation on Metal Surfaces, ACS Symposium Series 202, American Chemical Society, Washington, DC, 1982, p. 23.
[61] J.H. Bitter, K. Seshan, J.A. Lercher, J. Catal. 183 (1999) 336.
[62] J.R. Rostrup-Nielsen, J. Catal. 33 (1974) 184.
[63] B.C. Gates, J.R. Katzer, G.C.A. Schuit, Chemistry of Catalytic Processes, McGraw-Hill, New York, 1979 (Chapters 1 and 5).
[64] C. Naccache, in: J. Oudar, H. Wise (Eds.), Deactivation and Poisoning of Catalysts, Marcel Dekker, New York, 1985 (Chapter 5).
[65] W.G. Appleby, J.W. Gibson, G.M. Good, Ind. Eng. Chem. Process Des. Dev. 1 (1962) 102.
[66] H. Beuther, O.H. Larson, A.J. Perrotta, in: B. Delmon, G.F. Froment (Eds.), Catalyst Deactivation 1980, Stud. Surf. Sci. Catal., Vol. 6, Elsevier, Amsterdam, 1980, p. 271.
[67] A.G. Gayubo, J.M. Arandes, A.T. Aguayo, M. Olazar, J. Bilbao, Ind. Eng. Chem. Res. 32 (1993) 588.
[68] S.M. Augustine, G.N. Alameddin, W.M.H. Sachtler, J. Catal. 155 (1989) 217.
[69] M. Guisnet, P. Magnoux, Appl. Catal. 54 (1989) 1.
[70] F. Bauer, V. Karazirev, C. Vlaev, R. Hanisch, W. Weiss, Chemische Technik 41 (1989) 297.
[71] W.A. Grotten, B.W. Wojciechowski, B.K. Hunter, J. Catal. 138 (1992) 343.
[72] A. Bellare, D.B. Dadyburjor, J. Catal. 140 (1993) 510.
[73] M.A. Uguina, D.P. Serrano, R.V. Grieken, S. Venes, Appl. Catal. 99 (1993) 97.
[74] C. Li, Y. Chen, S. Yang, R. Yen, Appl. Surf. Sci. 81 (1994) 465.
[75] J.G. Buglass, K.P.D. Jong, H.H. Mooiweer (Eds.), in: Proceedings of the 120th National Meeting of the American Chemical Society on Analytic Studies of the Coking of the Zeolite Ferrierite, 20–24 August 1995, p. 631.
[76] D. Chen, H.P. Rebo, K. Moljord, A. Holmen (Eds.), Effect of coke deposition on transport and adsorption in zeolites studied by a new microbalance reactor, in: Proceedings of the 14th International Symposium on Chemical Reaction Engineering, Part B, 5–9 May 1996, p. 2687.
[77] M. Guisnet, P. Magnoux, D. Martin, in: C.H. Bartholomew, G.A. Fuentes (Eds.), Catalyst Deactivation 1997, Stud. Surf. Sci. Catal., Vol. 111, Elsevier, Amsterdam, 1997, p. 1.
[78] T. Masuda, P. Tomita, Y. Fujikata, K. Hashimoto, in: B. Delmon, G.F. Froment (Eds.), Catalyst Deactivation 1999, Stud. Surf. Sci. Catal., Vol. 126, Elsevier, Amsterdam, 1999, p. 89.
[79] H.S. Cerqueira, P. Magnoux, D. Martin, M. Gusinet, in: B. Delmon, G.F. Froment (Eds.), Catalyst Deactivation 1999, Stud. Surf. Sci. Catal., Vol. 126, Elsevier, Amsterdam, 1999, p. 105.
[80] S.E. Wanke, P.C. Flynn, Catal. Rev.-Sci. Eng. 12 (1975) 93.
[81] P. Wynblatt, N.A. Gjostein, Prog. Solid-State Chem. 9 (1975) 21.
[82] E. Ruckenstein, B. Pulvermacher, AIChE J. 19 (1973) 356.
[83] E. Ruckenstein, D.B. Dadyburjor, Rev. Chem. Eng. 1 (1983) 251.
[84] S.E. Wanke, in: J.L. Figueiredo (Eds.), Progress in Catalyst Deactivation, NATO Advanced Study Institute Series E, Marunus Nijhoff, Boston, 1982, p. 315.
[85] R.T. Baker, C.H. Bartholomew, D.B. Dadyburjor, Stability of Supported Catalysts: Sintering and Redispersion, Catalytic Studies Division, Catalytica Inc., Mt. View, California, 1991.
[86] C.H. Bartholomew, Catalysis, Specialist Periodical Report, Vol. 10, Royal Society of Chemistry, 1992.
[87] C.H. Bartholomew, Appl. Catal. 67 (1994) 1.
[88] C.H. Bartholomew, in: B. Delmon, G.F. Froment (Eds.), Catalysis Deactivation 1994, Stud. Surf. Sci. Catal., Vol. 88, Elsevier, Amsterdam, 1994, p. 1.
[89] C.H. Bartholomew, G.A. Fuentes (Eds.), Catalyst Deactivation 1997, Stud. Surf. Sci. Catal., Vol. 111, Elsevier, Amsterdam, 1997, p. 585.
[90] G.A. Fuentes, Appl. Catal. 15 (1985) 33.
[91] J.P. Bournonville, G. Martino, in: B. Delmon, G.F. Froment (Eds.), Catalyst Deactivation 1980, Stud. Surf. Sci. Catal., Vol. 6, Elsevier, Amsterdam, 1980, p. 159.
[92] G.A. Somorjai, X-ray and Electron Methods of Analysis, Plenum Press, New York, 1968 (Chapter 6).
[93] C.H. Bartholomew, W. Sorenson, J. Catal. 81 (1983) 131.

[94] S.R. Seyedmonir, D.E. Strohmayer, G.J. Guskey, G.L. Geoffroy, M.A. Vannice, J. Catal. 93 (1985) 288.
[95] D.L. Trimm, in: C.H. Bartholomew, J.B. Butt (Eds.), Catalyst Deactivation 1991, Stud. Surf. Sci. Catal., Vol. 68, Elsevier, Amsterdam, 1991, p. 29.
[96] A.G. Shastri, A.K. Datye, J. Schwank, Appl. Catal. 14 (1985) 119.
[97] L.L. Hegedus, K. Baron, J. Catal. 54 (1978) 115.
[98] J. Summers, L.L. Hegedus, Ind. Eng. Chem. Prod. Res. Dev. 18 (1979) 318.
[99] M.E. Dry, in: J. Anderson, M. Boudart (Eds.), Catalysis Science and Technology, Springer-Verlag, Berlin, 1981, p. 159.
[100] G.W. Huber, C.G. Guymon, B.C. Stephenson, C.H. Bartholomew, in preparation.
[101] T.P. Kobylinski, B.W. Taylor, J.E. Yong (Eds.), in: Proceedings of the SAE, Detroit, 1974.
[102] M. Shelef, H.S. Gandhi, Platinum Met. Rev. 18 (1974) 1.
[103] H.S. Gandhi, H.K. Stepien, M. Shelef, Mater. Res. Bull. 10 (1975) 837.
[104] C.H. Bartholomew, Ind. Eng. Chem. Prod. Res. Dev. 14 (1975) 29.
[105] R.W. Clark, J.K. Tien, P. Wynblatt, J. Catal. 61 (1980) 15.
[106] W.M. Shen, J.A. Dumesic, C.G. Hill, J. Catal. 68 (1981) 152.
[107] R.B. Pannell, K.S. Chung, C.H. Bartholomew, J. Catal. 46 (1977) 340.
[108] G. Lohrengel, M. Baerns, Appl. Catal. 1 (1981) 3.
[109] I. Qamar, J.G. Goodwin, in: Proceedings of the 8th Meeting of the American Catalytic Society, Paper C-22, Philadelphia, 1983.
[110] J.G. Goodwin, D.O. Goa, S. Erdal, F.H. Rogan, Appl. Catal. 24 (1986) 199.
[111] O. Watzenberger, T. Haeberle, D.T. Lynch, G. Emig, in: C.H. Bartholomew, J.B. Butt (Eds.), Catalyst Deactivation 1991, Stud. Surf. Sci. Catal., Vol. 68, Elsevier, Amsterdam, 1991, p. 441.
[112] M. Agnelli, M. Kolb, C. Mirodatos, J. Catal. 148 (1994) 9.
[113] H.C. Lee, R.J. Farrauto, Ind. Eng. Chem. Res. 18 (1989) 1.
[114] R.J. Farrauto, H.C. Lee, Ind. Eng. Chem. Res. 29 (1990) 1125.
[115] C.H. Bartholomew, Catal. Lett. 7 (1990) 27.
[116] F. Sperner, W. Hohmann, Platinum Met. Rev. 20 (1976) 12.
[117] N.L. Wu, J. Phillips, J. Phys. Chem. 89 (1985) 591.
[118] N.L. Wu, J. Phillips, Appl. Phys. 59 (1986) 769.
[119] N.L. Wu, J. Phillips, J. Catal. 113 (1988) 129.
[120] J.M. Hess, J. Phillips, J. Catal. 136 (1992) 149.
[121] A. Bielanski, M. Najbar, in: B. Delmon, G.F. Froment (Eds.), Catalyst Deactivation 1980, Stud. Surf. Sci. Catal., Vol. 6, Elsevier, Amsterdam, 1980, p. 127.
[122] N. Burriesci, F. Garbassi, M. Petrera, G. Petrini, in: B. Delmon, G.F. Froment (Eds.), Catalyst Deactivation 1980, Stud. Surf. Sci. Catal., Vol. 6, Elsevier, Amsterdam, 1980, p. 115.
[123] Y.L. Xiong, R. Castillo, C. Papadopoulou, L. Dada, J. Ladriere, P. Ruiz, B. Delmon, in: C.H. Bartholomew, J.B. Butt (Eds.), Catalyst Deactivation 1991, Stud. Surf. Sci. Catal., Vol. 68, Elsevier, Amsterdam, 1991, p. 425.
[124] R.J. Farrauto, M. Hobson, T. Kennelly, E. Waterman, Appl. Catal. 81 (1992) 227.
[125] P.L. Gai-Boyes, Catal. Rev.-Sci. Eng. 34 (1992) 1.
[126] B. Delmon, G.F. Froment (Eds.), Catalyst Deactivation 1994, Stud. Surf. Sci. Catal., Vol. 88, Elsevier, Amsterdam, 1994, p. 113.
[127] K.M. Erickson, D.A. Karydis, S. Boghosian, R. Fehrmann, J. Catal. 155 (1995) 32.
[128] B. Delmon, in: C.H. Bartholomew, G.A. Fuentes (Eds.), Catalyst Deactivation 1997, Stud. Surf. Sci. Catal., Vol. 111, Elsevier, Amsterdam, 1997, p. 39.
[129] N.B. Jackson, A.K. Datye, L. Mansker, R.J. O'Brien, B.H. Davis, in: C.H. Bartholomew, G.A. Fuentes (Eds.), Catalyst Deactivation 1997, Stud. Surf. Sci. Catal., Vol. 111, Elsevier, Amsterdam, 1997, p. 501.
[130] S.A. Eliason, C.H. Bartholomew, in: C.H. Bartholomew, G.A. Fuentes (Eds.), Catalyst Deactivation 1997, Stud. Surf. Sci. Catal., Vol. 111, Elsevier, Amsterdam, 1997, p. 517.
[131] A. Baranski, R. Dziembaj, A. Kotarba, A. Golebiowski, Z. Janecki, J.B.C. Pettersson, in: B. Delmon, G.F. Froment (Eds.), Catalyst Deactivation 1999, Stud. Surf. Sci. Catal., Vol. 126, Elsevier, Amsterdam, 1999, p. 229.
[132] C.A. Querini, F. Ravelli, M. Ulla, L. Cornaglia, E. Miro, in: B. Delmon, G.F. Froment (Eds.), Catalyst Deactivation 1999, Stud. Surf. Sci. Catal., Vol. 126, Elsevier, Amsterdam, 1999, p. 257.
[133] H.N. Pham, J. Reardon, A.K. Datye, Powder Technol. 103 (1999) 95–102.
[134] D.S. Kalakkad, M.D. Shroff, S. Köhler, N. Jackson, A.K. Datye, Appl. Catal. A: Gen. 133 (1995) 335–350.
[135] W.D. Callister Jr., Materials Science and Engineering: An Introduction, 5th Edition, Wiley, New York, 2000 (Chapter 13).
[136] R.L. Coble, W.D. Kingery, J. Am. Ceram. Soc. 39 (1956) 381.
[137] S.G. Deng, Y.S. Lin, AIChE J. 43 (1997) 505.
[138] S.G. Thoma, M. Ciftcioglu, D.M. Smith, Powder Technol. 68 (1991) 53.
[139] M. Bankmann, R. Brand, B.H. Engler, J. Ohmer, Catal. Today 14 (1992) 225.
[140] V.M. Kenkre, M.R. Endicott, S.J. Glass, A.J. Hurd, J. Am. Ceram. Soc. 79 (1996) 3045.
[141] H. Song, J.R.G. Evans, J. Am. Ceram. Soc. 77 (1994) 806.
[142] J. Werther, W. Xi, Powder Technol. 76 (1993) 39.
[143] B.L. Bhatt, Liquid Phase Fischer–Torpsch. II. Demonstration in LaPorte Alternative Fuels Development Unit, PR: PC A07/MF AO2, Performer: Air Products and Chemicals, Allentown, PA.
[144] H. Pham, A.K. Datye, The synthesis of attrition resistant slurry phase iron Fischer–Tropsch catalysts, in: Proceedings of the 217th National Symposium on Syngas Conversion to Fuels and Chemicals, Anaheim, CA, 21–25 March, American Chemical Society, Washington, DC, 1999.
[145] C.R. Bemrose, J. Bridgwater, Power Technol. 49 (1987) 97–126.

[146] M. Ghadiri, J.A.S. Cleaver, V.G. Tuponogov, J. Werther, Powder Technol. 80 (1994) 175.
[147] S.A. Weeks, P. Dumbill, Oil Gas J. (April) 16 (1990) 38.
[148] R. Zhao, J.G. Goodwin, K. Jothimurugesan, J.J. Spivey, S.K. Gangwal, Ind. Eng. Chem. Res. 39 (2000) 1155.
[149] P.K. Doolin, D.M. Gainer, J.F. Hoffman, J. Testing Evaluat. 21 (1993) 481.
[150] R. Oukaci, A.H. Singleton, D. Wei, J.G. Goodwin Jr., in: Proceedings of the 217th National Symposium on Syngas Conversion to Fuels and Chemicals, Anaheim, CA, 21–25 March, American Chemical Society, Washington, DC, 1999.
[151] M.J. Adams, M.A. Mullier, J.P.K. Seville, Powder Technol. 78 (1994) 5.
[152] G. Emig, F.G. Martin, Ind. Eng. Chem. Res. 30 (1991) 1110.